Materials Science and Engineering R 64 (2009) 1–31

Contents lists available at ScienceDirect

Materials Science and Engineering R

journal homepage: www.elsevier.com/locate/mser

Energetics of metal–organic interfaces: New experiments and assessment of the field

Jaehyung Hwang [1], Alan Wan [2], Antoine Kahn *

Department of Electrical Engineering, Princeton University, Princeton, NJ 08544, USA

ARTICLE INFO

Keywords:
Organic-metal interfaces
Molecular level alignment
Photoelectron spectroscopy

ABSTRACT

Considerable research and development means have been focused in the past decade on organic semiconductor thin films and devices with applications to full color displays, flexible electronics and photovoltaics. Critical areas of these thin films are their interfaces with electrodes, with other organic films and with dielectrics, as these interfaces control charge injection and transport through the device. Full understanding of the mechanisms that determine the electronic properties of these interfaces, i.e. the relative position of molecular levels and charge carrier transport states, is an important goal to reach for developing reliable device processing conditions. This report provides an extensive, although probably somewhat biased, review of polymer– and small molecule–metal interface work of the past few years, with emphasis placed specifically on (i) the electronic structure and molecular level alignment at these interfaces, (ii) the perceived differences between small molecule and polymer interfaces, (iii) the difference between organic-on-metal and metal-on-organic interfaces, and (iv) the role played by electrode surface contamination in establishing interface energetics. Environmental conditions, e.g. vacuum vs. ambient, are found to be critical parameters in the processing of polymer and small molecule interfaces with metals. With similar processing conditions, these two types of interfaces are found to obey very similar molecular level alignment rules.

© 2008 Elsevier B.V. All rights reserved.

Contents

* Corresponding author. Tel.: +1 609 258 4642; fax: +1 609 258 6279.
E-mail address: kahn@princeton.edu (A. Kahn).
[1] Currently: BASF, SE, D-67056, Ludwigshafen, Germany.
[2] Currently: Chem. & Chemical Bio. Dept., Rutgers University, New Brunswick, NJ, USA.

0927-796X/$ – see front matter © 2008 Elsevier B.V. All rights reserved.
doi:10.1016/j.mser.2008.12.001

1. Introduction

The past two decades have seen rapid progress in the development of organic semiconductor materials and organic-based devices, with ever improving performance in applications of light emission [1–7], large area flexible electronics [8–10], and photovoltaics (PV) [11–19]. High resolution full color flat panel displays with remarkable contrast and color properties, made of small molecule-based organic light emitting diodes (OLED), have been available in commercial products such as cell phones, camcorders or radios, and are now available in larger size, i.e. the 2007 XEL-1 11 in. Sony television screen. Durable, low power consumption, conformable lighting panels based on relatively simple structures of polymer light emitting diodes (PLED) are being developed as home consumer products [20]. Promising applications of organic electronics, exemplified by the organic field effect transistor (OFET), to drive flexible displays or control large-area applications for skin-like surfaces with a variety of sensors are being demonstrated [9,10,21]. Finally, the steady progress of light-conversion efficiency in all-organic, or hybrid organic–inorganic PV cells, reaching around 6.5% at the end of 2007 [17,18,22], gives reasonable prospect for large-area, inexpensive and efficient energy conversion application in the next couple of decades. It has been predicted that the market share for organic electronics will increase up to $20 billions by 2012 [23], and close to $100 billions by 2020 [20] with contribution from various applications.

Organic semiconductors have been hugely attractive for basic research and technological applications for several reasons. The first is perhaps the seemingly limitless diversity of tailored organic molecules, which is an unparalleled asset for a variety of (opto)-electronic applications. Molecular design can be directed to modify energy levels and gaps and optimize the color of absorbed or emitted photons, improve inter-molecular overlap and affect charge carrier transport in bulk or thin films, or simply adapt the molecular units to specific liquid or vacuum processing of organic thin films. The second reason is the ease with which one can stack, combine or mix molecular materials in a variety of device architectures. The closed-shell molecular structure of many of these materials enables retention of their intrinsic molecular electronic or optical properties in diverse structures, ranging from complex heterostructures to mixed-phase materials. This key property results from two fundamental, and related, characteristics: (i) the localized, "on molecule", nature of charge carriers and excitations in molecular and polymer semiconductors; and (ii) the absence of strong intermolecular bonding [24,25]. Molecules are bound by weak van der Walls (vdW) interaction, with limited intermolecular overlap of electronic wave functions. As a result, the electronic and optical properties of these materials are, to a first approximation, defined by those of the molecular moiety [26]. This is to be contrasted with inorganic semiconductors in which carriers are highly delocalized as a result of strong inter-atomic bonds and overlap of atomic wave functions. In these materials, defects like vacancies or interface misfits result in unsaturated dangling bonds, which introduce crippling deep electronic traps and optical recombination centers. Because vacancies or disorder do not break strong intermolecular bonds, such states do not form in organic molecular or polymer solids, at least as long as the chemical integrity of the molecule is preserved.

This unique "forgiving" quality of organic materials opens a range of possibilities for innovation on device architecture and fabrication techniques, which remain inaccessible to inorganic semiconductors. In most applications, molecular films are deposited without the constraints of lattice match and thermal budget, which greatly limit the fabrication of inorganic semiconductor structures. A classic example is the engineering via layer stacking of organic light emitting diodes (OLED) comprising multi-layers of hole or electron transport, blocking or electroluminescent materials (Fig. 1) [27–29], which facilitates the optimization of interface barriers, and leads to high-efficiency. This type of heterogeneous interface building between films of molecules with drastically different shapes and sizes is possible only because broken, or dangling, covalent bonds do not exist at these interfaces.

The flip side of this unparalleled flexibility is that excitation and transport processes in molecular materials are quite complex [24,30], far more so than in inorganic semiconductors where rigid band and single-particle approximations and charge carrier

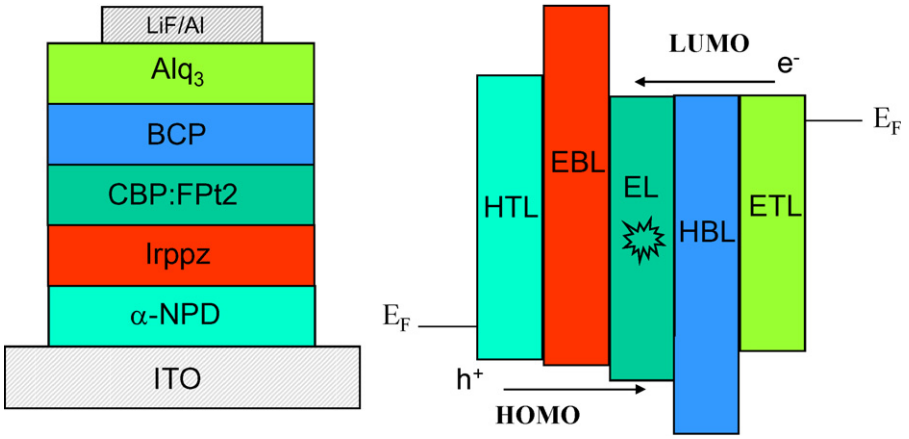

Fig. 1. Left: typical OLED made of stacked layers of hole and electron transport (HTL, ETL) and blocking layers (HBL, EBL), and electroluminescent (EL) layer. Right: corresponding energy diagram, showing approximate HOMO and LUMO positions (after [27]).

delocalization are commonly used to adequately describe electronic and optical processes [31]. The absence of strong intermolecular bonds and the weak overlap of electronic wave functions centered on adjacent molecules lead to "on-molecule" charge carrier localization and slow intermolecular transport by hopping. As a result, the electronic structure of these organic semiconductors generally corresponds to narrow molecular levels. Because of the slow charge hopping process, the strong polarizability of the π-electron system of the molecules, the relaxation of the charged molecules and the electron coupling to intra- and inter-molecular vibrations, the one-electron approximation and rigid band model universally used for wide band "delocalized" inorganic systems is no longer valid. Charge carriers are described in terms of polarons, the physics and transport of which are relatively complex and not always well understood.

Charge carrier injection and interface energetics, i.e. the relative molecular level energies across organic interfaces, are of paramount importance for all applications mentioned above. They ultimately determine key measures of device operation such as driving voltage and balance of electron and hole injection in OLEDs, or open circuit voltages in PV devices. Because of the thin-film architecture of most organic-based devices, interfaces are present within a few nanometers of any active layers, and this places considerable weight on their properties, integrity and stability.

For many reasons, contacts to molecular and polymer semiconductor films, which is the topic of this review, are complex and often difficult to understand and optimize. The first reason is that, on a conventional (mostly inorganic) semiconductor scale, the energy gaps of most of the organic materials used in OLEDs, OFETs and PV devices are large, generally in excess of 2.0–2.5 eV, making the fabrication of "good", i.e. ohmic, contacts for electron or hole injection difficult. The range of work functions of metals or conducting materials that can be practically used for making these contacts is also relatively limited. Electrode surface modification [32,33], the use of unconventional materials like high work function metal oxides [34], and interface doping of the organic films [35,36] for enhancing specific properties have therefore recently become important aspects of contact optimization. A second reason is the fragility of the molecular units against chemical reaction and the openness of the molecular matrix. Both lead to reacted and diffused interfaces, especially when contacts are deposited by conventional top vacuum evaporation. The impact of the resulting electronic states on the contact properties is generally unclear. Given the typical fabrication sequences used for organic devices, great care must also be taken to understand and eventually exploit the differences between organic-on-top and electrode-on-top interfaces. Finally, the most difficult aspect of these interfaces is that contact performance cannot be dissociated from bulk transport properties. Direct current–voltage (I–V) measurements of injection in an organic thin film are generally not sufficient to evaluate the contact, as the process of charge carrier transport, e.g. trap or space-charge limited, through the film is sometime difficult to assess. For example, a contact with injection barrier as large as 0.5–1.0 eV might function as an "ohmic" contact on a molecular film with low carrier mobility. Whether the current in a device is contact or transport limited is therefore not a trivial question to answer, and all means to investigate contacts and contact energy barrier must be employed, including interface spectroscopy of molecular levels.

The fact that organic-on-electrode and electrode-on-organic interfaces are relevant and can be fabricated without major impact on the quality of the organic semiconductor itself is a great advantage from the view point of understanding and controlling the mechanisms that dominate the electronic structure of these boundary regions. It allows working on these interfaces from various angles, for example by surface modification to increase or decrease the electrode work function before depositing the organic material by soft vacuum evaporation or spin-coating. It allows as well the investigation of the effects of electrode surface contamination on the interface barrier. This point is of the utmost importance for a technology that, *in fine*, will rely on low vacuum or ambient processing conditions that are far from the conditions generally required for interfaces with inorganic crystalline semiconductors. Thus organic interfaces of many different types, involving small molecules or polymers, metals or conducting dielectrics, organic-on-electrode or electrode-on-organic, and processed under widely different conditions, have received considerable attention and have been the topic of multiple spectroscopy and charge transport investigations.

This review article provides an up-to-date, although admittedly not unbiased, assessment of the current understanding of energetics at organic–electrode interfaces. We start with a short review of the main models that have been put forth to explain various observations at such interfaces, and a brief account of the experimental methods used in our work. We then review our current understanding of interfaces between both polymer and small molecule films and electrodes (metal and non-metal), and conclude with a unified picture of these seemingly different interfaces.

2. Current understanding of metal–organic interfaces

2.1. Standard models

The interface electronic structure of a typical metal–(organic) semiconductor interface is shown in Fig. 2. Important electronic levels are the electrode Fermi level (E_F); the semiconductor highest occupied and lowest unoccupied molecular orbitals (HOMO, LUMO), i.e. the hole and electron transport levels, respectively; and the vacuum level (E_{vac}) of each material. The work function of the electrode (ϕ_M), and the ionization energy (IE) and electron

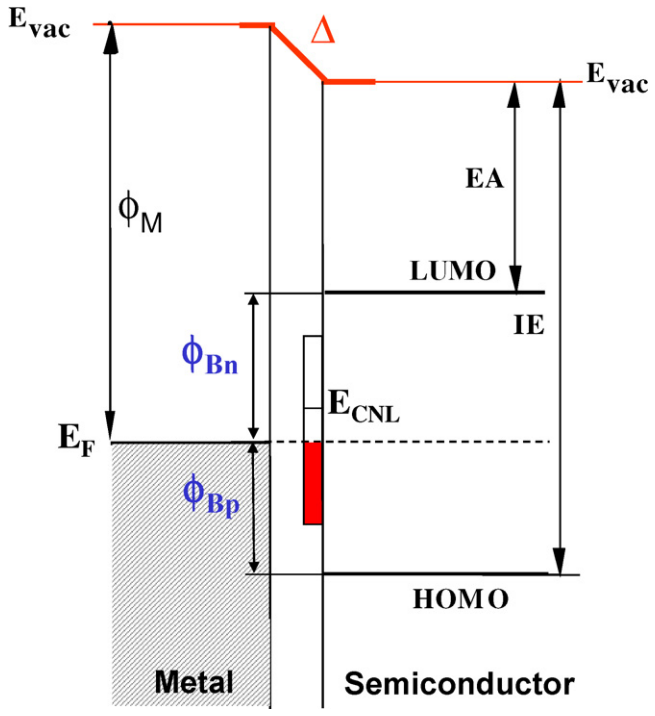

Fig. 2. Electronic structure of a typical (organic) semiconductor–metal interface, showing relevant energy levels on both sides, the electron affinity (EA) and ionization energy (IE) of the semiconductor, the interface dipole Δ, the interface density of gap states and charge neutrality level E_{CNL}, and the electron and hole injection barriers ϕ_{Bn} and ϕ_{Bp}.

affinity (EA) of the semiconductor are defined as the energy difference between vacuum and Fermi levels for the metal, and vacuum level and HOMO or LUMO, respectively, for the semiconductor. The density of interface gap states, D_{is}, the nature of which will be discussed in Section 2.1.2.2, is schematically represented between the HOMO and LUMO, and the interface shift between the vacuum levels of the two materials, or interface dipole barrier, is denoted as Δ. Central to charge carrier injection through the interface are the electron and hole injection barriers, ϕ_{Bn} and ϕ_{Bp}, respectively. Standard metal–semiconductor interface treatments [37–39] lead to the following equations for the electron injection barrier:

$$\phi_{Bn} = S(\phi_M - EA) + (1 - S)E_{CNL} \quad (1)$$

$$S = \frac{1}{1 + 4\pi e^2 D_{is}\delta} \quad (2)$$

where most of the parameters have been defined above, δ is the effective metal–semiconductor distance, and E_{CNL} is the charge neutrality level of the interface states. If the interface E_F is above (below) E_{CNL}, the net charge in the interface states is negative (positive), and a dipole Δ with corresponding sign develops across the interface.

One of the most important aspects of such an interface is the dependence of the injection barriers on the nature and work function of the electrode, which is the central topic of this paper. Eq. (1) gives an explicit, if over-simplified, dependence of the barrier on the metal work function, which naturally depends on the nature of the interface through the density of interface states D_{is}. We rapidly review several basic models that address this dependence, before examining the actual situation with small molecule and polymer films.

2.1.1. Interfaces free of gap states

2.1.1.1. The Schottky–Mott model. The Schottky–Mott limit assumes a vanishingly small density of interface states D_{is}, corresponding to a non-interactive metal–semiconductor interface. In such a case, the position of the molecular levels with respect to the electrode E_F follows from vacuum level alignment, or $\Delta = 0$, in Fig. 2. Specifically, the electron injection barrier ϕ_{Bn} is equal to the difference between the electrode work function ϕ_M and the organic electron affinity EA. Alternatively, the hole injection barrier is equal to $\phi_{Bp} = IE - \phi_M$. A useful parameter to describe the dependence on the barrier on the electrode is the interface parameter S (Eq. (1)) defined as the derivative of the electron barrier with respect to the electrode work function: $S = d\phi_{Bn}/d\phi_M$. In the Schottky–Mott limit, *as long as the electrode Fermi level overlaps with the semiconductor gap*, i.e. $EA < \phi_M < IE$, S should be equal to unity [37,39]. We stress the importance of this condition. Understandably, the interface will depart from the simple Schottky–Mott picture if the work function of the electrode decreases to reach the semiconductor EA, leading to a large electron transfer from the metal to the LUMO of the organic film. A similar situation, with charge transfer from the organic HOMO to the metal, occurs as the electrode work function increases and reaches the semiconductor IE. There have been recent reports of such charge transfer and Fermi level pinning when the electrode Fermi level approaches the limits of the polymer gap. Interpretations based on E_F alignment with the polaron state of the organic material [40] or E_F penetration in the density of states tailing in the gap [41] have been given, and will be discussed in Section 4.3.

Returning to the common type of non-interactive interfaces described in this section, the extensive body of work done on organic interfaces in the past decade shows specifically that interfaces formed by spin-coating polymer films on metal electrodes closely follow the Schottky–Mott limit (Fig. 3) [42,43] and that interfaces formed by evaporating small molecule films on (ambient or controlled atmosphere) contaminated metal surfaces approach this limit [44]. On the other hand, metal-on-polymer and metal-on-small molecule [45] interfaces, generally made by vacuum thermal evaporation of the metal, as well as small molecule-on-clean metal interfaces [46–49], depart from vacuum level alignment. The reasons for these differences are discussed in the following sections.

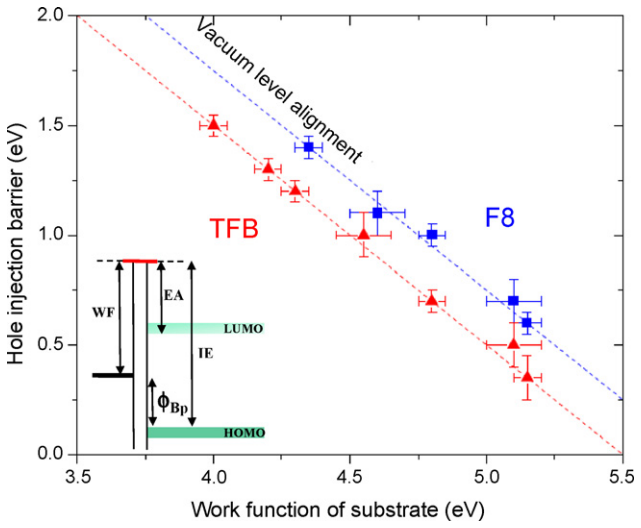

Fig. 3. Hole barrier measured by UPS at polymer-on-substrate interfaces plotted as a function of substrate work function for poly(9,9′-dioctylfluorene) (F8) (square) and poly(9,9′-dioctylfluorene-*co*-bis-*N*,*N*′-(4-butylphenyl)diphenylamine) (TFB) (triangle). The data points fit on the vacuum level alignment, or Schottky–Mott, line. Inset: schematic energy diagram showing the organic semiconductor HOMO, LUMO, ionization energy (IE), electron affinity (EA), the electrode work function (WF) and the hole injection barrier (ϕ_{Bp}).

2.1.1.2. Reorganization of surface metal electronic structure: the "pillow effect". When an atom or molecule is deposited on a metal surface, the Coulomb repulsion between its electronic density and the surface metal electrons locally suppresses the tail of electron wave function that spills into vacuum. This phenomenon systematically reduces the work function of the metal. The extent of the reduction depends sensitively on the component of the work function attributed to the original tailing of electrons into vacuum from the atomically clean metal surface, and is generally larger for large work function noble metals. Work function changes due to adsorbates on metal surfaces have been extensively investigated, in particular for noble gases on series of metals [50]. The idea was re-introduced in the past decade as part of the effort to understand organic molecule–metal interfaces [51,48,52], and is commonly known as "pillow effect". Work function reductions of clean noble metal surfaces, e.g. Au, by 0.5–1.0 eV upon deposition of conjugated molecules have been reported and partially attributed to this phenomenon. Note that the reduction in work function associated with this effect should not be viewed as resulting from the formation of an interface dipole, as is with charge transfer (see the next section), but simply as the modification (or suppression) of the "external" surface component of the work function of the metal.

2.1.2. Interfaces dominated by gap states

In contrast to the situation encountered in the Schottky–Mott limit, the presence of a significant density of interface states D_{is} (Fig. 2; Eq. (2)) is known to limit the range of interface Fermi level excursion, and to eventually lead to E_F pinning when D_{is} is large

enough. A huge number of investigations on this topic, focusing mainly on inorganic semiconductor interfaces, date back to the 1970–1990s and have been reviewed in many comprehensive articles and books [38,39,53,54]. For the purpose of the present review, it is sufficient to recall that a density of interface states in excess of $\sim 5 \times 10^{13}\,\mathrm{cm}^{-2}\,\mathrm{eV}^{-1}$ with energy in the gap of the semiconductor has a significant impact on the position of the interface E_F. Eqs. (1) and (2) show that S approaches zero for large D_{is}, leading to a Fermi level position (and injection barrier) defined by the charge neutrality level (E_{CNL}) of the interface states.

2.1.2.1. Defect and chemistry-induced gap states. Interface states have diverse origins. One is chemical and corresponds to the formation of chemical bonds and/or defects between the semiconductor and the metal [53,55–57]. A frequent occurrence when a metal is vacuum-evaporated on a molecular film is the formation of metal-induced defects in the organic material, or of an organometallic complex, which exhibit filled or empty electronic states that overlap with the original gap of the semiconductor [58–60]. A clear example is the extensively investigated reaction between aluminum or magnesium and tris-(8-hydroxyquinoline)aluminum (Alq_3) [61], which leads to the formation of gap states that pin the Fermi level in the upper part of the Alq_3 gap [62–64]. Experience shows that such reaction products can also be found at interfaces formed by molecular evaporation on a reactive metal, even though these organic-on-metal interfaces are generally considered as more abrupt and less reactive than their metal-on-organic counterparts [63]. Defect- or reaction-induced states, which are omnipresent at inorganic semiconductor interfaces, do therefore play a significant role at reactive organic interfaces as well.

2.1.2.2. The induced density of interface states (IDIS). At a metal–semiconductor interface, the metal electron wave function tails into the semiconductor [65–67]. The penetration depth is short and depends exponentially on the semiconductor band gap [67]. The proximity of the metal surface and the overlap between continuum of metal states and semiconductor states broaden the latter, and induces a density of interface states in the gap of the semiconductor, known as metal-induced gap states (MIGS) or induced density of interface states (IDIS) [65–68]. This concept, which was developed and extensively researched three decades ago for inorganic semiconductor interfaces, was recently applied to weakly interacting organic molecular interfaces [69,70]. The molecular levels of interface molecules in close proximity to the metal surface are broadened and form the IDIS. The charge neutrality level E_{CNL} is calculated by integrating the local density of states in the IDIS and imposing that the total number of electrons up to E_{CNL} equals the number of electrons in the neutral molecule. Thus the total charge in the IDIS is zero if the Fermi level precisely aligns with E_{CNL}, and positive or negative if it is below or above, respectively.

As the metal–organic interface is formed, electron redistribution across the interface hinges on the magnitude of the metal work function relative to the E_{CNL} position (below vacuum level). If the work function is smaller, electron transfer takes place from the metal to the IDIS, setting up an upward dipole barrier at the metal–organic interface, i.e. the vacuum level shifts upward from the metal to the organics. This dipole narrows the energy difference between E_F and E_{CNL}. If the work function is larger, both electron transfer and the dipole are in opposite directions. The extent to which E_F aligns with, or diverges from, E_{CNL} (i.e. by changing the metal work function) depends on the density of states at or around E_{CNL}, as stipulated by Eqs. (1) and (2). As the density increases, S decreases and the interface Fermi level position and associated injection barriers become increasingly independent of the metal work function. Typical densities of IDIS around the E_{CNL} for interfaces between perylenetetracarboxylic dianhydride (PTCDA) or dicarbazolyl-biphenyl (CBP) have been calculated to be of the order of a few $10^{14}\,\mathrm{cm}^{-2}\,\mathrm{eV}^{-1}$ [69,70], clearly sufficient to affect the electronic structure of the interface. Note that the effective "distance" between the semiconductor and the metal, which appears as δ in Eq. (2), also plays an important role in the strength of this pinning, and will be discussed again in Sections 4.5 and 5.2 in the context of interface formation on contaminated or modified metal surfaces.

Two points need to be stressed to conclude this section. The first is that the IDIS and E_{CNL} concepts, as developed by Vazquez et al. [69] are applicable to weakly interacting organic–metal interfaces only. It is clear that they do not account for dominant mechanisms related to chemistry, i.e. bonding, and electronic defects formed at reactive interfaces where chemistry- or defect-induced states control the Fermi level position. Second, an extension of the IDIS model to incorporate the effect of work function reduction by molecular adsorption, i.e. the "pillow effect" (see above), in a self-consistent fashion was recently put forth [71] and improved the consistency of the model.

2.1.3. Basic observations on interface processing-dependent energetics

2.1.3.1. Small molecule vs. polymer interfaces. An examination of the basic experimental results obtained in the past decade on the energetics of small molecule-on-metal and polymer-on-metal interfaces shows that the former generally depart from the Schottky–Mott limit whereas the latter closely follow it. In other words, many investigations of small molecule-on-metal interfaces show significant vacuum level shift at the interface, and hole or electron injection barriers that do not vary with a unity slope with the metal work function, i.e. $S < 1$ in Eqs. (1) and (2) [45,46,72]. On the other hand, vacuum level alignment and $S \sim 1$ is obtained for polymer-on-metal interfaces [73]. We stress that organic-on-metal interfaces are being considered here, as metal-on-organic interfaces bring other issues that will be discussed in Sections 4.4 and 5.1.

As will be amply detailed in the following sections, the difference between small molecule-on-metal and polymer-on-metal interfaces does not stem from intrinsic differences between small molecule and polymer semiconductors, but rather from the specific conditions under which their interfaces with metals are formed. A large number of small molecule-on-metal interfaces investigated in the past decade were formed by vacuum evaporation on clean metal surfaces, in an effort to unravel the intrinsic mechanisms that control the electronic structure without interference from contamination effects. These interfaces exhibit therefore energetics that result from an intimate contact between metal surface and organics, including the formation of gap states (related to defects or IDIS) and the "pillow effect" described above. These mechanisms generally result in a significant interface dipole (Δ up to 1.0–1.5 eV) [46,72], partial pinning of the Fermi level and, thus, departure from the Schottky–Mott limit [45]. Polymer-on-metal interfaces, on the other hand, are formed by spin-coating the organic compound from solution on metal surfaces which, by necessity, are exposed to at least controlled atmosphere, e.g. nitrogen, and more generally to ambient, as well as to the polymer solvent. These surfaces are contaminated and their "starting" work function is already modified with respect to that of the clean counterparts. Furthermore, this surface contamination acts as a separation layer placed between the metal and the organic film, and attenuates the organic–metal interaction. These surfaces closely approach the Schottky–Mott limit [73], and will be reviewed in Section 4.2.

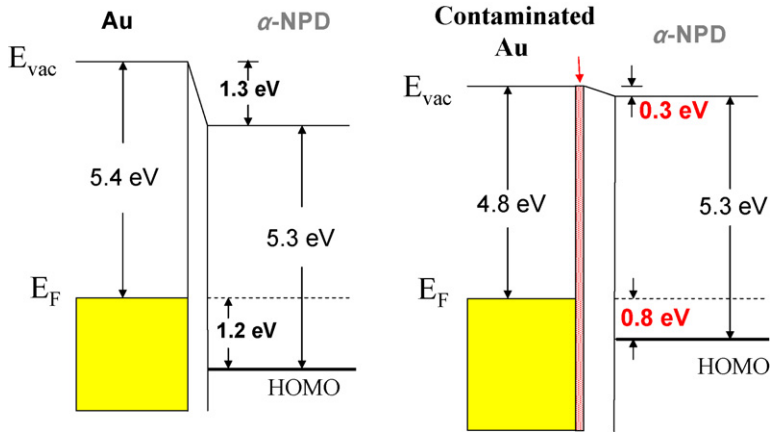

Fig. 4. Electronic structure of interfaces formed by vacuum evaporation of *N*;*N*^{I}-diphenyl-*N*,*N*^{I}-bis(1-naphthyl)-1,10-biphenyl-4,4^{II}-diamine (α-NPD) on atomically clean Au (left) and Au exposed to ambient atmosphere (right). The contamination layer is shown in red. The work function of the contaminated Au surface is 0.6 eV smaller than that of the atomically clean surface (after [44]). (For interpretation of the references to color in this figure legend, the reader is referred to the web version of the article.)

Another interesting observation, which will be the topic of Section 5.2, is that small molecule–metal interfaces formed by vacuum evaporation of molecules on metal surfaces pre-exposed to controlled atmosphere, or ambient air, do approach the Schottky–Mott limit far closer than their ultra-clean counterparts [44]. Near vacuum level alignment is obtained at most of these interfaces, defining a different electronic structure than would be obtained with the same organic compound deposited on the ultra-clean metal surface. This situation leads to interesting, and somewhat counter-intuitive, results whereby smaller hole injection barriers into a specific molecular material is obtained with a smaller work function contaminated metal surface then with its larger work function ultra-clean counterpart (Fig. 4) [44]. Therefore, these interfaces resemble the Schottky–Mott interfaces obtained with polymer films.

2.1.3.2. Organic-on-metal vs. metal-on-organic. Another important processing issue for organic–metal systems is the sequence of formation of the interface. It is expected, and often verified, that metal atoms evaporated from a hot source on a soft organic molecular or polymer film induce significant damage and diffusion into the organic film [59,74]. On the other hand, organic molecules vacuum-deposited (from a relatively low temperature source) or spin-coated on a cold metal surface are expected to form an abrupt interface. Chemical reaction is possible in this case as well [75], but its spatial extend is expected to be confined to the interface layer. A topic of scientific as well as technological interest is therefore whether, given a specific pair of metal and organic material, the organic-on-metal interface does or does not exhibit the same energetics and charge carrier injection properties than its metal-on-organic counterpart [76]. Fig. 5 shows the example of two metal/organic/metal structures, i.e. Al/Alq_3/Al [75] and Pt/poly(9,9′-dioctylfluorene-*co*-bis-*N*,*N*′-(4-butylphenyl)diphenylamine)/Pt [77], or Pt/TFB/Pt, that behave quite differently. The former shows symmetric electron injection from top and bottom Al electrodes, whereas the latter shows higher hole injection from the bottom Pt contact. The Alq_3 structure was fabricated in ultra-high vacuum (UHV), both organic-on-metal and metal-on-organic involve clean electrodes, and the energetics

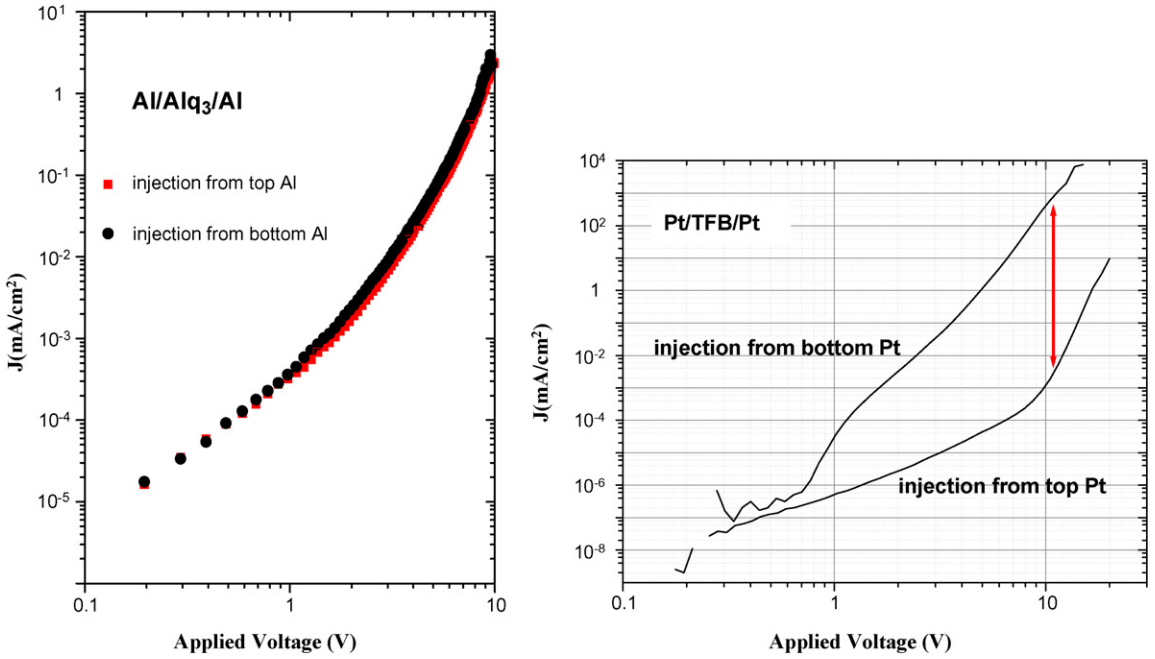

Fig. 5. Current density injected from top (evaporated) and bottom electrodes in Al/Alq_3/Al [75] (left) and Pt/TFB/Pt [77] (right) structures. Currents in Alq_3 and TFB are unipolar electron and hole currents, respectively.

of both interfaces are controlled by the Al-Alq_3 chemical reaction [64], leading to identical bottom and top barriers. On the other hand, the TFB structure was formed by spin-coating the polymer on a Pt surface exposed to ambient, and by evaporating the top Pt electrode on the polymer film in high vacuum. Thus the top contact involves a clean metal, whereas the bottom interface is formed on a contaminated surface. In line with the initial discussion presented in Section 2.1.3, these two interfaces exhibit different energetics and different charge injection properties. A more detailed analysis of these issues and of the models used to understand these structures will be presented in Section 5.

3. Experimental methods

The main experimental techniques used to investigate the energetics of organic interfaces are direct and inverse photoemission spectroscopies (PES, IPES) (for general reviews of the techniques, see [78] and references therein), and current–voltage (I–V) measurements of electron and hole injection into simple organic structures. PES and IPES provide information on the energy distribution of occupied and unoccupied states at the surface and interface of the film, respectively, whereas I–V measurements show how the interface electronic structure translates in actual charge carrier injection and transport. All the spectroscopy and I–V experimental results presented in this work were obtained in situ on highly controlled systems: (i) small molecule and metal films formed and analyzed in UHV; (ii) polymer films formed in inert atmosphere (N_2) and transferred to UHV without ambient exposure; (iii) interfaces formed on electrode surfaces, prepared in UHV or controllably contaminated.

The valence photoemission work involved a specific brand of PES, i.e. ultra-violet photoemission spectroscopy (UPS), done with helium discharge lamps, using two specific radiation lines: HeI, $h\nu$ = 21.22 eV and HeII, $h\nu$ = 40.8 eV [79]. Photo-excited electrons were detected with cylindrical mirror analyzers. The energy resolution of these UPS measurements was 100–150 meV. The core level photoemission work was done with standard non-monochromatized X-ray sources providing two different radiation lines: Al Kα, $h\nu$ = 1486.6 eV and Mg Kα, $h\nu$ = 1253.6 eV and the same detectors as for UPS. The energy resolution of the XPS measurements was ~800 meV.

IPES was done in the isochromat mode, using a low energy electron gun and a fixed-energy photon detector based on a design by Avci et al. [80]. This apparatus has been amply described elsewhere [81]. In IPES, incident electrons with controlled kinetic energy (5–15 eV) penetrate the solid above the vacuum level and decay in an empty state. The energy is released in the form of a photon, which is captured by the detector. The number of photons collected as a function of electron energy provides the density of unoccupied states in the solid under investigation. The ratio between photon flux per incident electron in IPES and electron flux per incident photon in PES is $(q/k)^2$, where q and k are photon and electron wave vectors, respectively [82]. Given that the photon and electron energies involved in these experiments are of the order of 10 eV, this ratio is of the order of 10^{-5}. This emphasizes the difficulty of the IPES experiment, which suffers from low yield and signal-to-noise ratio, and thus requires relatively large incident electron currents. Considerable care was taken in our measurements to prevent damage by electrons to the organic films. Electrons beam were defocused, currents were kept to a minimum and data recording times were reduced as well. Averaging data from different spots on the surface of the organic film was found to be an effective way to operate. The resolution of the IPES measurements presented here was ~450 meV.

A detailed description of UPS and IPES is beyond the scope of this review, and the interested reader will find many useful

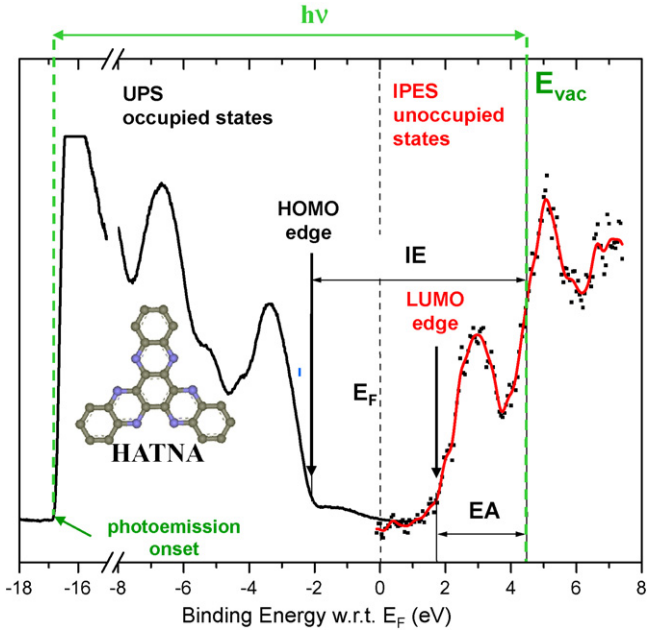

Fig. 6. Combined UPS and IPES spectra from a 6 nm film of HATNA deposited on Au [83]. The chemical structure of the molecule is shown in inset. The photoemission onset, the vacuum level (E_{vac}), the HOMO and LUMO edges, and the ionization energy (IE) and electron affinity (EA) are indicated.

references to these techniques in the literature. However, some basic principles of the analysis must be given here in order to clearly understand the UPS and IPES data presented below for the interested reader. Fig. 6 shows the composite UPS and IPES spectra collected from a thin film of the small molecule hexaazatriaaphthylene (HATNA) deposited on a gold (Au) surface [83]. The left spectrum (black) is the UPS spectrum of occupied states, and the right spectrum (red) is the IPES spectrum of the unoccupied states. These spectra were taken in the same chamber on the same organic film, and the common energy scale was obtained by aligning the Fermi steps measured with both techniques on the same Au surface. Both UPS and IPES spectra consist in a series of features corresponding to single or multiple occupied and unoccupied molecular levels, respectively. In the process of photoemission, a hole is left on the positively charged molecule. In the final state, the hole induces (i) electronic polarization on the neighboring molecules (energy of the order of 1–1.5 eV) [30,84,85], (ii) molecular relaxation of the charged molecule (energy of the order of 100–200 meV) [85] and (iii) "lattice" relaxation of the surrounding molecules (energy of the order of 10 meV) [85]. Whether these energies are reflected in the photoemission spectra depends on the times scales of the processes. It is generally assumed that the largest and fastest, i.e. the one corresponding to electronic polarization, is included, but that the slower mechanisms (ii) and (iii) are not. However, their energies are relatively small with respect to the first one, and the UPS spectrum of the HOMO is therefore taken to provide a fairly accurate measure of the nearly fully relaxed positive polaron (the missing pieces are the molecular and lattice relaxation components). This is important, as it shows that the photoemission (UPS) measurement is highly relevant to the determination of the hole transport level in the molecular solid [45]. Similarly, and assuming similar time scales and energies for the IPES process, the IPES spectrum of the LUMO is taken to provide a fairly accurate measure of the nearly fully relaxed negative polaron, and thus a measure of the electron transport state [86–88]. The energy gap between these two states is known as the single particle gap, or transport gap (E_t) [30,86,87], which should be contrasted with the

optical gap (E_{opt}), i.e. the energy required to create a neutral excitation, or exciton, on the molecule. The difference between E_t and E_{opt} is the energy necessary to break the exciton pair and produce separated free electron and free hole, and is therefore the exciton binding energy [81,85].

The determination of E_t from the UPS and IPES experimental data is not a trivial matter, and hinges upon the interpretation of the origin of the width of the spectroscopic features, e.g. the HOMO in Fig. 6, and the magnitude of effects such as polarization at the surface vs. in the bulk of the film. Hill et al. [85] developed a specific procedure to determine the mean E_t, which involved taking the gap between the peak positions of the HOMO and LUMO, and correcting this gap for the difference between surface and bulk electronic polarization. For most organic materials, the identification of the HOMO and LUMO peak positions requires theoretical support of the type described in the next section. Other procedures have been proposed, which emphasize the edge of the HOMO and LUMO features [89,90], which are clearly outlined in Fig. 6. We note that Hill et al.'s procedure has led to the determination of exciton binding energies in organic small molecule solids ranging from 0.5 eV to more than 1 eV [85] (and ~0.5 eV in polymers, see below), in accord with previous evaluations [86,87,91,92]. On the other hand, procedures based on edge-to-edge determination of the mean transport gap lead to far smaller binding energies (0.1–0.4 eV) [89,90]. For the sake of clarity, we point out that papers on electronic structure of organic thin films and interfaces often refer to the edge of the density of occupied and unoccupied states measured with UPS and IPES as *the* HOMO and LUMO levels. This is clearly an approximation, given that the width of these spectroscopic features is the result of several different mechanisms (see discussion in Section 4.1.2). Yet the confusion between molecular level and edge of the density of state is often made and, in a sense, is accepted by the community.

In that respect, and for the purpose of this work and nearly all similar spectroscopy analysis of organic interfaces that focus on the charge carrier injection barrier, which is a very different issue than the exciton binding energy, the convention has been to take the onset of the filled and empty states on the UPS and IPES spectra, i.e. the intercept between the tangent of the onset feature and the base-line of the spectrum, as the position of the HOMO and LUMO, respectively. To distinguish it from E_t, the energy gap between these edges will be referred to as $E_{edge\text{-}to\text{-}edge}$ in this review. This gap is illustrated in Fig. 6, which shows a view of the gap area of HATNA and associated onset positions. The justification for this procedure is not entirely solid for organic materials, because the origin of the broadening of the molecular features, and thus of the physical meaning of the onset, is still a matter of research and controversy [90]. However, it constitutes a well-defined procedure that we will apply herein when talking about injection barriers.

The secondary electron cut-off (left most part of the UPS spectrum of Fig. 6) provides a direct measure of the vacuum level (E_{vac}) of the sample [93]. By definition, the cut-off is at the minimum energy an electron can have and still escape from the solid, i.e. E_{vac}. The spectroscopic features of the UPS spectrum (HOMO, HOMO-1, etc.) are the signatures of electrons that have absorbed one photon with energy $h\nu$ and escaped elastically from the solid. Therefore, the proper relative position of E_{vac} with respect to these features is obtained by translating the energy position of the secondary cut-off by the photon energy (see Fig. 6). The position of E_{vac} (at 4.45 eV in Fig. 6) can then be used to determine the ionization energy IE (6.58 eV), the work function (4.45 eV) and electron affinity EA (2.76 eV) of the solid. The key elements of the electronic structure of the organic materials with regards to interface energetics and charge carrier injection and transport can therefore be fully determined. A representation of IE, EA and the edge-to-edge gap determined by UPS and IPES for a number of organic compounds, including those mentioned in this review, is presented in Fig. 7. The chemical structures of the latter are shown in Fig. 8.

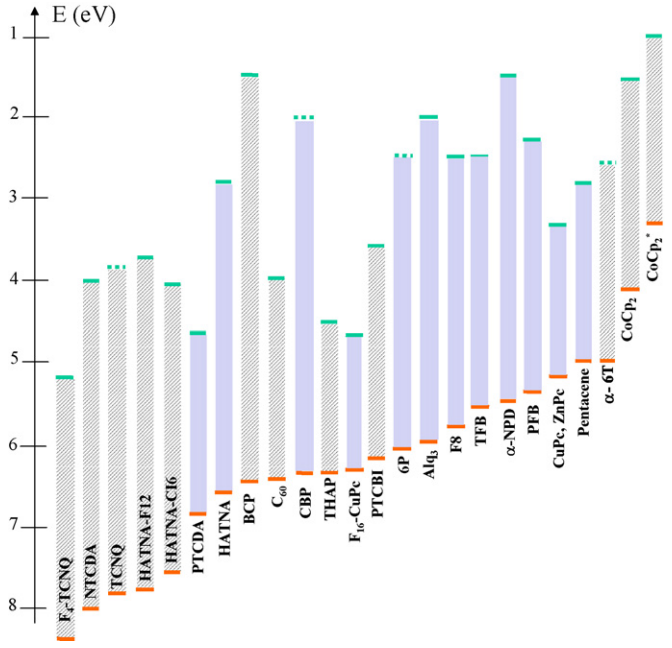

Fig. 7. Energy position of the HOMO (bottom line) and LUMO (top line) edges of various organic small molecule and polymer films, determined by UPS and IPES respectively. Corresponding IEs and EAs are obtained on the vertical energy scale (E_{vac} = 0). See also Table 1. Dashed top lines correspond to LUMO positions indirectly obtained from the HOMO position, the optical gap and an approximate exciton biding energy for the material. Compounds specifically mentioned in this review are colored in light blue. (For interpretation of the references to color in this figure legend, the reader is referred to the web version of the article.)

Finally, an essential component of work on the electronic structure of organic interfaces is the probing of charge carrier injection into, and transport through, the organic thin film itself. Interface electronic structure and charge transport are sufficiently complex that current–voltage (I–V) characteristics are the key that allows one to understand the impact of the energetics on the device performance. In the work described in this review, most of the spectroscopic data were complemented with I–V characteristics recorded in situ, i.e. in vacuum or in N_2, without exposure of the device to ambient. The devices are generally simple electrode/organic/electrode structures designed with two overriding concerns: (i) to fabricate the interface of interest according to the method used to form the same interface investigated via UPS or IPES; and (ii) to build a unipolar device in order to test the injection and transport of one type of carrier at a time. Fig. 5 illustrates results from such devices, whereby Al produces a very large hole injection barrier on Alq_3, insuring that the observed current is an electron current only, regardless of the polarity of the bias; and Pt produces a very large electron injection barrier on TFB, insuring that the observed current is a hole current only.

4. Energetics of polymer–electrode interfaces

One of the key difficulties in using polymers in organic electronic devices, rather than small molecules, is the lack of flexibility for fabricating multi-layered structures with functionalities distributed to different layers. Indeed, polymers face solubility issues that greatly complicate multi-layer fabrication. As mentioned at the beginning of this review, the ability to stack multi-layer structures of hole or electron transport, blocking or electroluminescent materials (Fig. 1) has been at the core of the

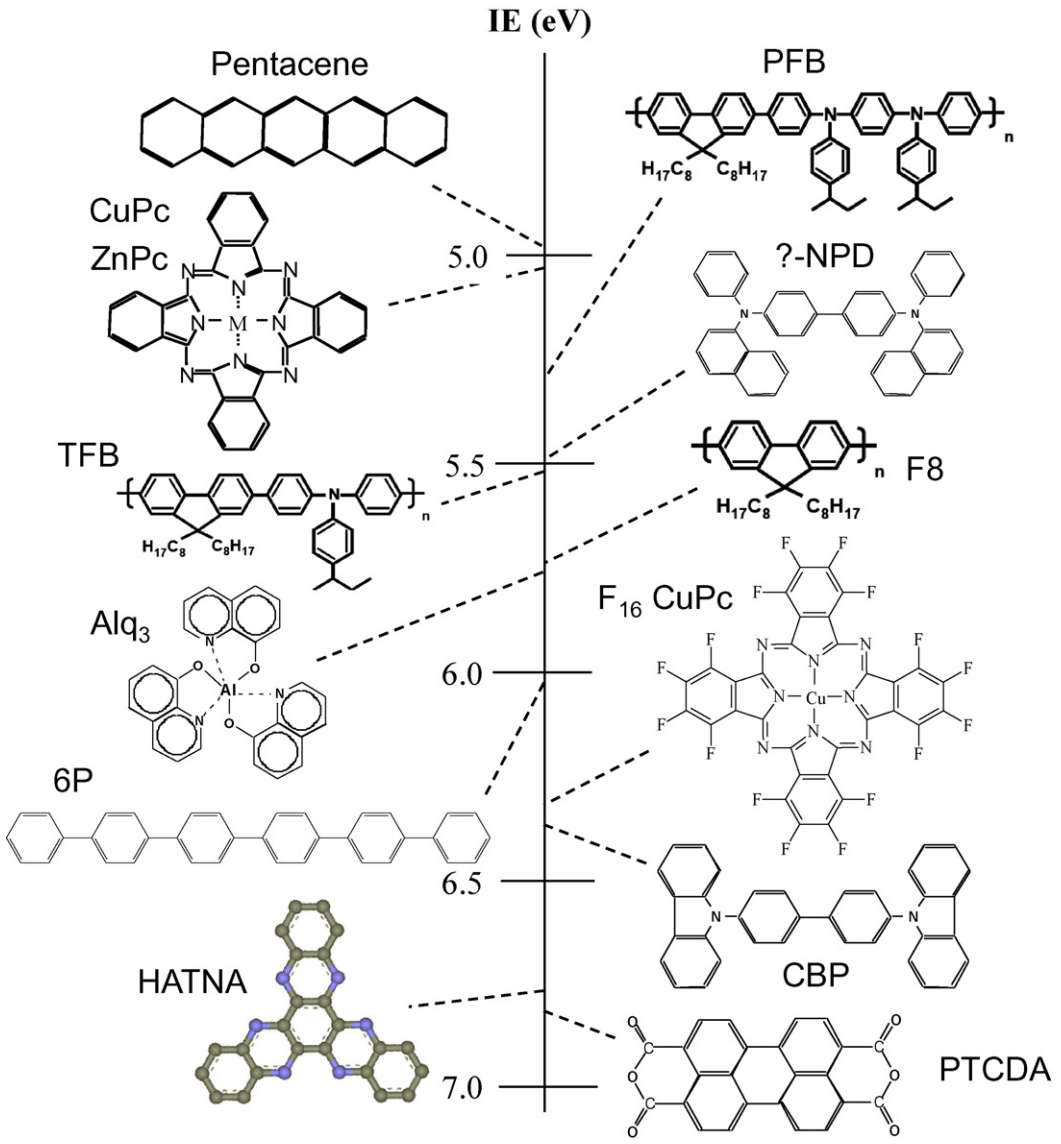

Fig. 8. Chemical structure of all the compounds mentioned in this review. In ascending order of ionization energy: pentacene; copper phthalocyanine (CuPc); poly(9,9′-dioctylfluorene-*co*-bis-*N*,*N*′-(4-butylphenyl)-bis-*N*,*N*′-phenyl-1,4-phenylenediamine) (PFB); *N*;*N*^{I}-diphenyl-*N*,*N*^{I}-bis(1-naphthyl)-1,10-biphenyl–4,4^{II}-diamine (α-NPD); poly(9,9'-dioctylfluorene-*co*-bis-*N*,*N*′-(4-butylphenyl)diphenylamine) (TFB); poly(9,9′-dioctylfluorene) (F8); tris-(8-hydroxyquinoline)aluminum (Alq_3); para-sexiphenyl (6P); dicarbazolyl-biphenyl (CBP); per-fluorinated copper phthalocyanine (F_{16}-CuPc); and perylenetetracarboxylic dianhydride (PTCDA).

success of high efficiency small molecule OLEDs [27–29]. With simpler polymer structures, all the charge distribution in the device and the balance between electron and hole injection and transport are inevitably controlled by a single active layer and its interfaces with the anode and cathode. The energy and the density of the electron and hole transport states, and their relative positions across the electrode–organic interfaces are therefore of paramount importance for the performance of the device.

The determination of interface energetics by traditional techniques such as photoemission spectroscopy or charge carrier transport measurements is more difficult for polymer films than for small organic molecular films for at least two reasons. The first is the disordered and mixed nature of the polymer materials. Polymer electronic states can be thought of as more delocalized along the chains than the highly localized states of a small π-conjugated molecule material. Yet, the complex morphology of the film and local structure of, and defects in, the chains, which are always difficult to control over significant dimensions, greatly affect the electronic and optical properties of these materials [94,95]. They are a source of additional difficulty in the interpretation of electronic structure and transport properties. Inter-chain transport is also limited by hopping. Structural disorder and the mix of extended and localized states are reflected in the width of the spectroscopic features, and complicate therefore the interpretation of the spectroscopic data. A detailed analysis of spectroscopic features, aided by theoretical computations of the density of states of the material, is necessary to identify the electronic levels of the materials [96].

The second reason that makes the determination of polymer interface energetics more difficult is a practical one: while (sub)monolayer films of small molecules can be routinely deposited by vacuum evaporation and investigated with interface-sensitive spectroscopy, it is difficult to form ultra-thin polymer films (≤2–3 nm thick) by spin-coating, and this limits access to polymer-on-electrode interfaces for investigations of energetics via standard techniques, i.e. UPS or XPS. The interpretation of data, generally collected at the surface of thicker (10–15 nm) polymer films, must therefore be carefully considered in order to extrapolate the results to the interface of interest.

Yet, much work has been done on polymer interfaces, predominantly by the group of Salaneck and co-workers [42,96,97], and a general understanding of the mechanisms that control their electronic structure has begun to emerge. We do not claim to review this large body of work here, but we attempt to illustrate the state of understanding of polymer–electrode interfaces with examples relating to three compounds: poly(9,9′-dioctylfluorene) (F8, also known as PFO) and two fluorene-arylamine copolymers, poly (9,9′-dioctylfluorene-*co*-bis-*N*,*N*′-(4-butylphenyl) diphenylamine) (TFB) and poly(9,9′-dioctylfluorene-*co*-bis-*N*,*N*′-(4-butylphenyl)-bis-*N*,*N*′-phenyl-1,4-phenylenediamine) (PFB) (Fig. 8). F8 has been extensively studied [95,97,98] and is a candidate for commercial applications. TFB has recently been shown to improve the efficiency of polymer light emitting devices [99]. These materials are first investigated via UPS and IPES to define their transport states. The data are complemented by theoretical calculations performed at the density functional theory (DFT) level by the group of Brédas. The energetics of interfaces formed between these polymers and various substrates are then investigated. Vacuum level alignment, i.e. the Schottky–Mott limit, is found to hold at most polymer-on-electrode interfaces, in good agreement with earlier results for other polymer–metal interfaces [42,100]. Deviations from that limit are observed when E_F of the electrode approaches the HOMO or LUMO states. On the other hand, the energetics of electrode-on-polymer interfaces are found to depart from the Schottky–Mott limit, presumably due to the strong metal–organic interactions that dominate these intimate interfaces, as alluded to in Section 2.1.3.1.

4.1. Electronic structure: polymer charge transport levels

4.1.1. Ionization energy, electron affinity, transport gap and exciton binding energy

An example of combined UPS and IPES spectra recorded from the surface of a 160 Å thick F8 film spin-coated on the conducting doped polymer poly(3,4-ethylenedioxythiophene)–poly(styrenesulfonate) (PEDOT–PSS) is given in Fig. 9. The photo-current and incident current densities during the measurements are generally limited to 1 nA/mm^2 and 0.1 μA/mm^2 for UPS and IPES, respectively, to prevent charging. The work function of the PEDOT–PSS substrates, measured on a control sample prepared at the same time and under the same conditions as the substrates used for the polymer films, and exposed to the polymer solvent prior to measurement, is 5.15 ± 0.05 eV. The ionization energy, electron affinity, and edge-to-edge gap, $E_{edge\text{-}to\text{-}edge}$, measured between the onsets of occupied and unoccupied states (=IE − EA), of the three polymers are summarized in Table 1.

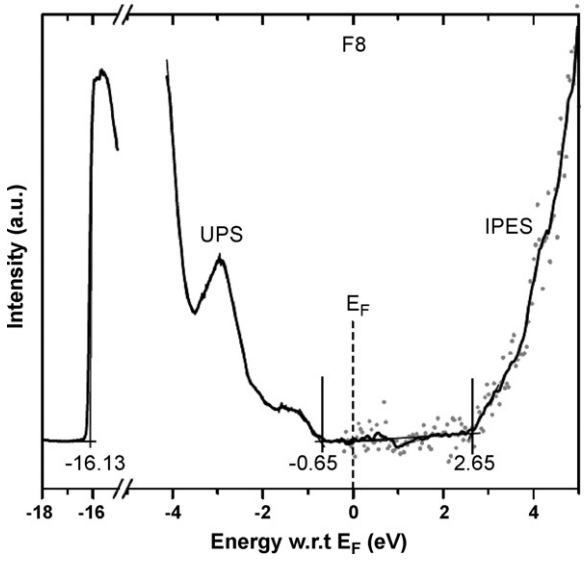

Fig. 9. Combined UPS and IPES spectra recorded from a ∼16 nm thick F8 film spin-coated on PEDOT–PSS. Approximate energy position of the edges of filled and empty states, along with the photoemission onset, are given relative to E_F (after [41]).

Table 1
Ionization energy (IE), electron affinity (EA) and edge-to-edge gap ($E_{edge\text{-}to\text{-}edge}$) of various compounds used in this review. Variations of these values of 0.2–0.3 eV from experiment to experiment and group to group are not uncommon, and are due to a range of factors, such as molecular orientation [139] and film morphology.

	IE (eV)	EA (eV)	$E_{edge\text{-}to\text{-}edge}$ (eV)	Reference
F8	5.75	2.50	3.25	[41]
TFB	5.50	2.45	3.05	[41]
PFB	5.30	N/A	N/A	[41]
Alq_3	5.80	2.2	3.6	[49]
α-NPD	5.2–5.5	1.5	∼3.8–4.0	[49]
CuPc	5.2	3.4	1.8	[49,157]
Pentacene	5.0–5.1	2.70–2.85	2.20–2.30	[158–160]
F_{16}-CuPc	6.3	4.5	1.8	[49]

The width of the UPS and IPES peaks and the featureless aspect of the IPES spectrum in Fig. 9 prevent a precise identification of the molecular levels of the materials. A detailed computation of the occupied and unoccupied density of states is therefore required to better understand the electronic structure of the materials. The computations presented here were performed by the group of Brédas, and details pertaining to the calculation can be found elsewhere [41]. F8 and TFB were modeled as infinite chain consisting of four monomeric units in the supercell under periodic boundary conditions (F8 and TFB monomer units are shown in Fig. 8). A standard procedure involving (i) the convolution of the calculated density of states with a Gaussian function of full-width-at-half-maximum (FWHM) equal to 0.55 eV (σ = 0.23 eV); and (ii) an expansion of the energy scale by a factor of 1.2 followed by a uniform shift representing solid-state polarization to align theoretical and experimental peaks was used to simulate UPS and IPES spectra [101,102].

The comparison between calculated and measured UPS and IPES spectra of F8 and TFB (Fig. 10) allows a clear identification of all molecular level positions. The agreement between theory and experiment, in particular in the expanded gap region, leads to a reliable determination of the gap. Both peak-to-peak and edge-to-edge gaps are presented, as well as associated values of ionization energy (IE) and electron affinity (EA). Note that $E_{edge\text{-}to\text{-}edge}$ should also be equal to the sum of the electron and hole injection barriers from any given electrode.

As discussed above, the difference between E_t and E_{opt} represents the exciton binding energy in the material. Optical absorption and electron energy loss spectroscopy, EELS (Fig. 11), both provide a measure of E_{opt}. The former identifies the onset of optical absorption with the formation of a (Frenkel) exciton on a neutral molecule [94], and gives values of 2.95 and 2.85 eV for E_{opt} of F8 and TFB, respectively [103]. In the latter, electrons with fixed incident energy (here 30 eV) are back-scattered from the organic surface, where they loose energy to a number of excitation, in particular the formation of excited electron–hole pairs on the neutral molecule [91]. EELS gives onset values of 2.85 and 2.7 eV for the F8 and TFB optical gaps, respectively, in relatively good agreement with the optical absorption values [104].

Using the peak-to-peak energy gaps (Fig. 10) and the procedure developed by Hill et al. for molecular film [85], the single particle gap E_t, adjusted for surface vs. bulk polarization effects [105], is found equal to 3.5 eV for F8 and 3.25 eV for TFB. Using the E_{opt} obtained from optical absorption, the estimated exciton binding energies for F8 and TFB are 0.55 eV and 0.4 eV, respectively. These numbers should be considered as estimates with fairly large error

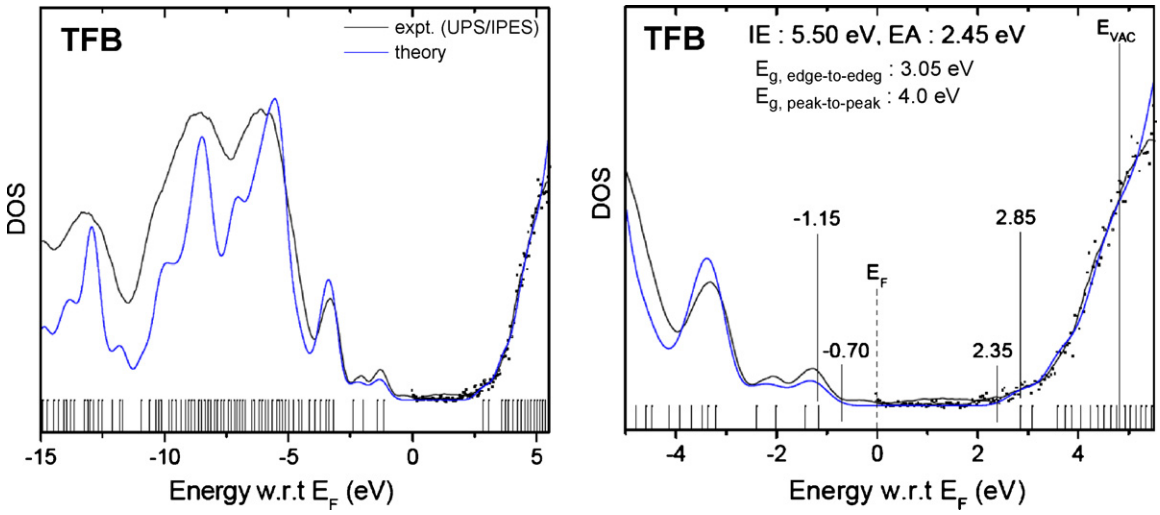

Fig. 10. (Left) Comparison between measured DOS (black line) and calculated DOS (blue line) for TFB. Calculated molecular levels are represented by short vertical bars. The calculated density of states was first convolved with a Gaussian function of FWHM = 0.55 eV (σ = 0.23 eV) and the energy-level scale was then expanded by a factor of 1.2. (Right) Magnified view of the gap area. The position of peak and edge of the HOMO and the LUMO are indicated in the figure (after [41]). (For interpretation of the references to color in this figure legend, the reader is referred to the web version of the article.)

bars of 0.2–0.3 eV, but give the sense that exciton binding energies in these polymer films, while significantly smaller than in small molecular systems [85,87,88,91,106,107], are nonetheless significant. Similar values have been found for other polymer semiconductors, such as poly(5,7-dodecadiyne-1,12 diol-bis(4-butoxycarbonylmethylurethane)) [108].

4.1.2. Width of the HOMO feature

In order to understand an important aspect of Fermi level pinning at polymer–electrode interfaces, which will be presented in Section 4.2, we look here at the width of the spectroscopic feature that represents the (occupied) frontier states. We contend that Fermi level pinning at energies significantly above and below the HOMO and LUMO levels determined by spectroscopy is due to the density of occupied and unoccupied states, respectively, tailing into the gap of the material.

The density of frontier states of an organic material has usually been assumed to be Gaussian. Fig. 12 shows the top of the occupied states of F8 and TFB measured by UPS [104]. The leading edge of the two HOMO features is well fitted with a Gaussian curve with σ equal to 0.27 ± 0.2 eV and 0.22 ± 0.1 eV for F8 and TFB, respectively. Care must be taken, since these values are not obtained from fitting on a single orbital peak, but on the overlap from multiple molecular states, especially for TFB where the HOMO and HOMO-1 are relatively close to each other (Fig. 10). However, the error is minimized by fitting only the lower binding energy part of the slope of the HOMO edge. In the present case, the HOMO width of both materials remains constant as a function of temperature, as shown by the UPS data of Fig. 13, suggesting that static, rather than dynamic, disorder plays the key role in the feature width [104].

In order to extract a Gaussian width representative of the hole state, the experimental spectrum must be corrected for experimental broadening, broadening due to surface vs. bulk polarization [105], and vibrational (phonon) coupling [109]. The broadening due to the instrumental resolution (σ_{inst}) can be estimated from the width of the Fermi step measured on a clean metal surface (Fig. 12c). Since this width should only be a few kT, most of the width of the Fermi step spectrum is due to instrumental broadening. Assuming a Gaussian broadening, the σ_{inst} measured from the Fermi step of clean Au is 0.11 ± 0.05 eV.

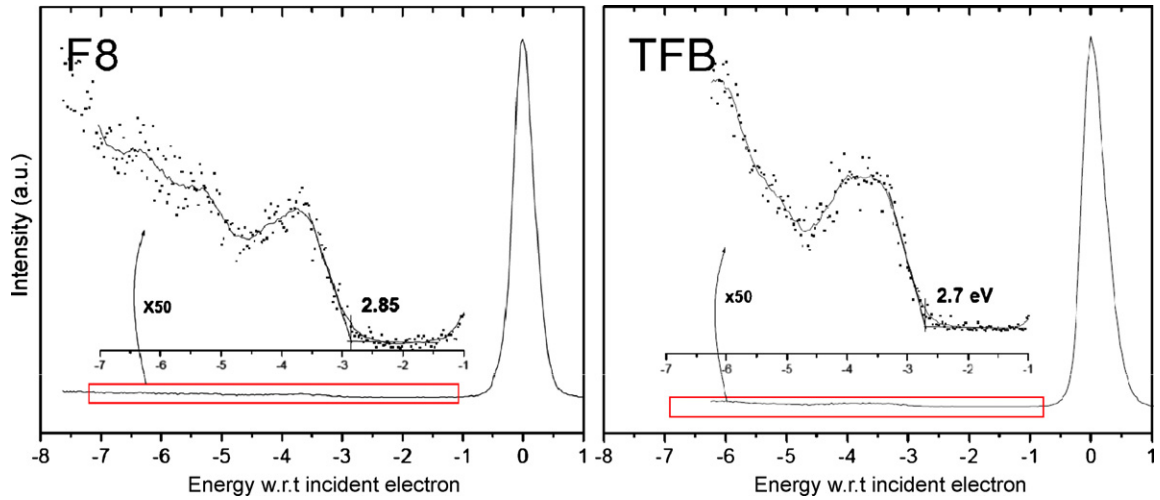

Fig. 11. Electron energy loss spectra from F8 and TFB. The right part of each graph shows the elastic peak, i.e. lossless reflection of incident electrons (FWHM ~0.5 eV). The magnified left part is the loss spectrum. The onset of the loss features, which provides a measure of the optical gap, is at 2.85 eV for F8 and 2.7 eV for TFB (after [104]).

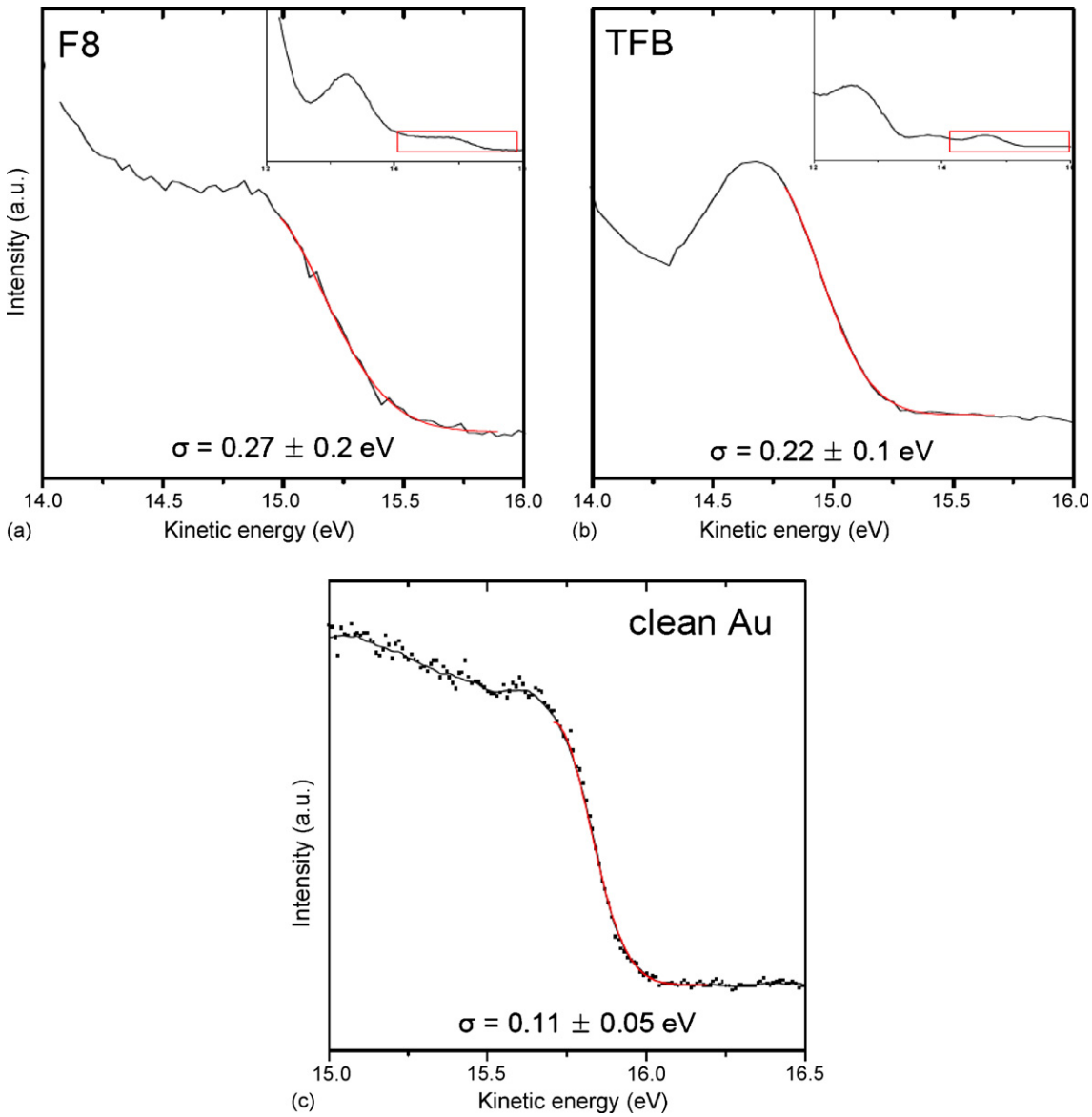

Fig. 12. Top of the occupied states of (a) F8 and (b) TFB, and (c) Fermi step of sputter-cleaned Au [104]. The edge of each peak is fitted with Gaussian peak, which yields a width of 0.27 eV and 0.22 eV for HOMO of F8 and TFB, and 0.11 eV for the Fermi step of Au.

The difference between electronic polarization induced during the photoemission process at the polymer surface and in the bulk also contributes to broadening (σ_{surf}). Indeed, the smaller polarization at the surface leads to valence levels shifted to higher binding energy with respect to valence levels corresponding to electrons originating from deeper in the organic solid [110]. Thus the finite elastic mean free path of the photoemitted electron yields an overlap of progressively shifted spectra from the top, second, third, etc., layers, which results in a broadened molecular feature. A precise measurement on the difference between surface and bulk polarization on the polymers used for this study has not been reported, but various studies of small molecule films give a conservative value of ~0.2–0.3 eV distributed over the first three or four layers [110,111]. Using an elastic mean free path δ = 10 Å and a simple exponential decay of the intensity of the signal from sub-surface layers according to $\exp(-\delta/d)$, where d is the depth of the layer, a simulation (not shown here) yields a Gaussian broadening σ_{surf} = 0.11–0.12 eV for both F8 and TFB.

The broadening due to vibrational coupling (σ_{vib}) corresponds to a loss of photo-excited electron energy to various vibrational states of the molecule. Lacking direct measurements on F8 and TFB, this broadening is estimated here based on the energy levels and the intensity ratio of higher order excited states of small molecules like copper phthalocyanine (CuPc) and pentacene, for which the energy separation between neighboring excited states was measured to be ~0.15 eV [109] and ~0.16 eV [112], respectively. Assuming similar vibrational coupling, σ_{vib} = 0.05–0.1 eV can be estimated for our purpose. Note that the various components of the broadening discussed so far are not likely to play a role in the transport, as they are exclusively the result of the UPS measurement.

The overall shape of the HOMO measured by UPS is the convolution of all the broadening factors, and the width of the Gaussian corresponding to the HOMO is the root mean square (RMS) of the width of each process including the instrumental broadening, expressed as follows:

$$\sigma_{UPS} = \sqrt{\sigma^2_{Material} + \sigma^2_{Measurement}} = \sqrt{\sigma^2_{Material} + (\sigma^2_{Inst} + \sigma^2_{Suf} + \sigma^2_{vib})}$$

where $\sigma_{Material}$ is the intrinsic width of the Gaussian corresponding to the material. Although the estimation of the broadening introduces large error bars due to the approximations explained

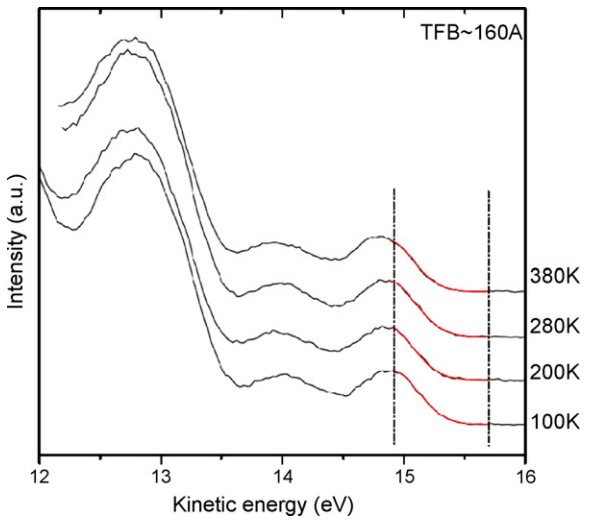

Fig. 13. TFB occupied states measured by UPS at different temperatures [104]. The change in the width of the Gaussian fit to the HOMO with different temperatures is negligible.

above, it is nevertheless useful in order to estimate the "real" Gaussian width (σ_{Material}) of the HOMO of the polymer. Subtracting all the broadening due to the measurement, σ_{Material} is estimated to be 0.20 ± 0.01 eV for F8 and 0.13 ± 0.01 eV for TFB, respectively.

σ_{Material} stems mainly from static disorder, which includes differently oriented polymer chains and local variations in material density, or defects and variations in the conjugation length of the chains. All these phenomena lead to a spread in polarization energy, which affects not only the UPS data, but the charge carrier transport levels as well, and thus is conceptually important for the interface electronic structure. Other components of σ_{Material} are intra- and inter-molecular band dispersion [113,114]. The latter is expected to be small (~10 meV) [25] for an amorphous polymer film, in which only weak intermolecular coupling is present. The former, on the other hand, can be significantly larger due to lengthy conjugation along the backbone of the chain. The calculated overall intra-molecular energy band dispersions for the two polymers discussed in this section, based on four monomeric units (4F for F8 and FTFT for TFB), are shown in Fig. 14. The shaded area below the Fermi level shows that the valence band is more dispersive in F8 (~0.15 eV) than in TFB (~0.1 eV). Further calculations on isolated oligomers indicate that: (i) the reorganization energy due to the presence of a charge is larger on TFB than on F8; and (ii) that stronger localization of the charge occurs on the triphenylamine unit of TFB, whereas the charge is more delocalized on the backbone of the chain in F8 (Fig. 15). Theory suggests therefore that intra-chain hole transport should be superior in F8 than in TFB. The fact that hole transport is measured to be superior in TFB than in F8 [115] presumably stems from the fact that inter-chain hopping dominates the process in these mostly amorphous disordered systems.

Finally, quantitative measurements of the density of state (DOS) at frontier orbitals have been reported for both polymer [116] and small molecule films [117,118]. While the DOS is complex in the case of the polymer, i.e. poly(p-phenylene vinylene) (PPV), it is relatively well approximated with a Gaussian function with $\sigma = 0.19$ eV, not unlike in the crude evaluation presented above. Furthermore, the analysis shows that a significant DOS extends several 100 meV into the gap, an important point to which we will come back in Section 4.3.

4.2. Energy level alignment at polymer-on-metal interfaces

This section focuses on interface energetics of the three polymers spun on various substrates. In most polymer electronic

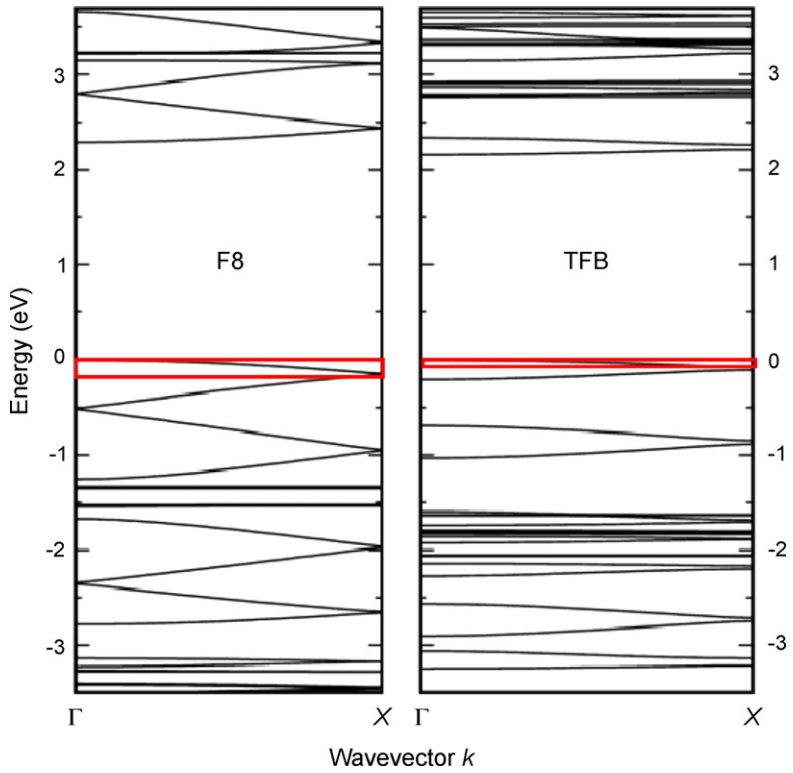

Fig. 14. Calculated band structure of F8 (left) and TFB (right) along the ΓX direction [161]. The calculation was performed on four monomer units of each polymer. The red box in each graph shows the dispersion of the HOMO in each polymer. (For interpretation of the references to color in this figure legend, the reader is referred to the web version of the article.)

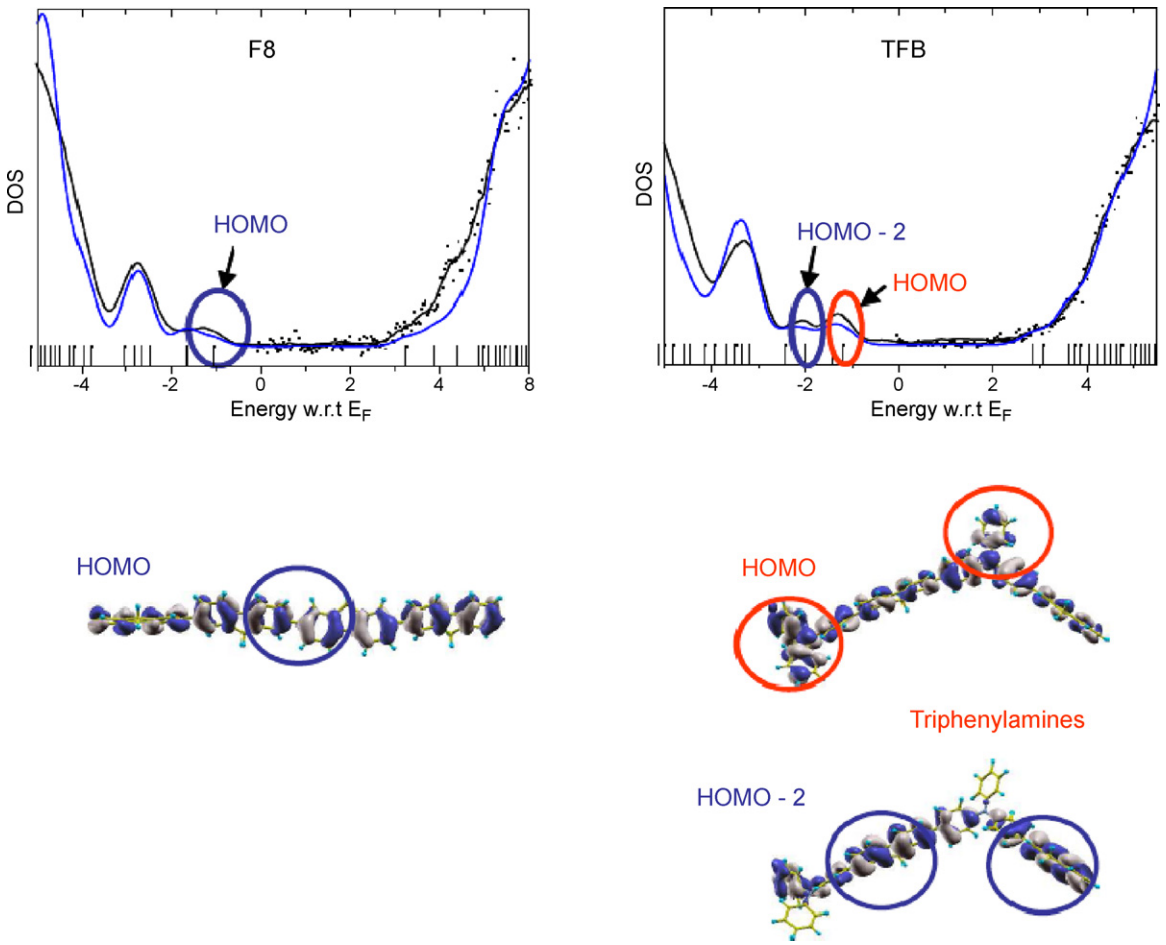

Fig. 15. The calculated HOMO orbital of (left) F8 and (right) TFB. The HOMO of F8 is more delocalized along the chain, while that of TFB is localized on triphenylamine [161].

device fabrication, the anode material (hole injecting side) rather than cathode material (electron injecting side) is used as the starting substrate. This is essentially due to two fact: (i) the cathode needs to be a low work function electrode, which has so far been best achieved by a last-step vacuum evaporation of metals like Al, Ca; (ii) the high work function anode materials of choice, e.g. PEDOT–PSS or indium tin oxide (ITO), cannot be easily deposited on top of the polymer film, and thus are used as starting bottom substrates. For these reasons, we choose here PEDOT–PSS, ITO and Au, well-known high work function materials, as our model substrates. UV-ozone treated ITO and Au, which exhibit higher work functions that their non-treated counterparts, are also occasionally used. All the experiments are performed according to the procedures described in Section 3. In each case, the interface molecular level alignment was determined by: (i) measuring the substrate work function *after* exposure to the polymer solvent; (ii) spin-coating a 8–10 nm polymer film in N_2; and (iii) UPS measurement after protected transfer (no ambient exposure).

The results for the polymer interfaces are summarized in Figs. 16 and 17, which show the HOMO edge and vacuum level positions of F8, TFB and PFB films with respect to the substrate vacuum and Fermi levels, as measured by UPS *at the surface of the film*. Each panel includes the work functions of the substrate and the energy difference between E_F and HOMO. The IE of each polymer, is indicated (see also Fig. 7 and Table 1). Of these 10 interfaces, seven show vacuum level alignment with the substrate, as measured at the surface of the polymer film. Three, i.e. TFB/PEDOT–PSS, PFB/PEDOT–PSS and PFB/ozone-treated Au, exhibit an apparent down shift of the substrate E_{vac} into the polymer film.

The seven cases of vacuum level alignment are in line with the results of several previous investigations on similar polymer/electrode systems, which have already shown Schottky–Mott limit behavior [42,100], unlike small organic molecules vacuum-deposited on clean metal surfaces, which can form interfaces with a dipole barrier of up to 1 eV [49,72,119,120]. The latter will be rapidly reviewed in Section 5.1. The Schottky–Mott limit for polymer-on-electrode interfaces is rationalized by considering that these interfaces are far from the intimate contact interface formed between a small molecule film and an atomically clean metal surface in UHV, where the mechanisms outlined in Sections 2.1.1 and 2.1.2, i.e. charge exchange and dipole, control the interface energetics. Polymer films are spun from solution in a nitrogen or ambient environment on a substrate surface that is generally contaminated with hydrocarbons and/or oxides. Note that when a small molecule film is vacuum-deposited on an ambient-exposed metal substrate, the interface dipole barrier decreases significantly with respect to that obtained on the same but atomically clean metal, and the interface energetics approach the Schottky–Mott limit for this semiconductor/metal interface (Section 5.2) [44]. Similarly, the unavoidable contamination layer that exists between the polymer film and the metal surface reduces the polymer–substrate interaction and allows the Schottky–Mott limit. Given that the polymers used in this study are not (intentionally) doped, we assume that the energy position of the vacuum level and of the HOMO are constant throughout the polymer film from the interface to the surface, i.e. flat band across the polymer film. In this case, the interface hole injection barrier, which is defined as the difference between E_F and HOMO at the

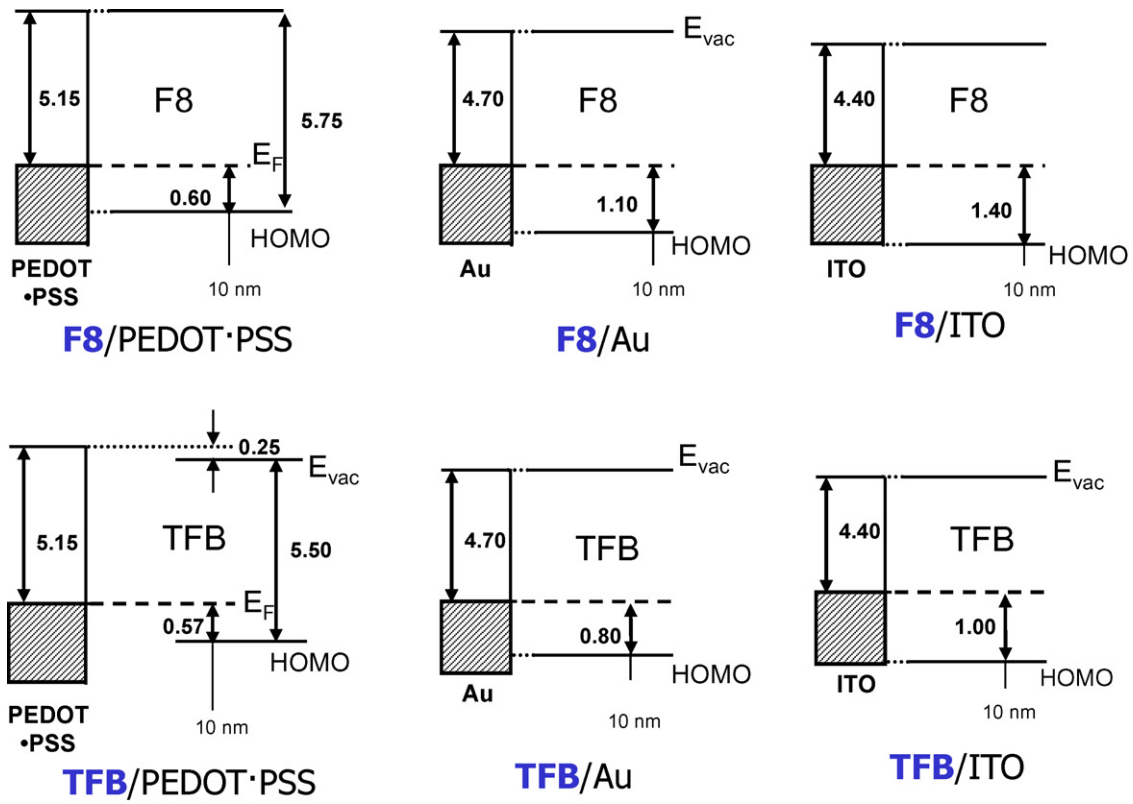

Fig. 16. Energy positions of the vacuum level and HOMO level of F8 and TFB measured at the surface of a 10 nm thick polymer film spin-coated on various substrates. The substrate work function, E_F and bulk E_F–HOMO are indicated in each case (after [41]).

interface, is simply the difference between the polymer IE and the work function of the substrate (Figs. 16 and 17).

The three interfaces, i.e. TFB/PEDOT–PSS, PFB/PEDOT–PSS and PFB/ozone-treated Au exhibit a significant shift between the vacuum level of the substrate, measured before spin-coating the polymer film, and the vacuum level measured *at the surface* of the polymer film. Note that these three cases occur for the polymers with "medium" and "small" IE, i.e. 5.50 eV and 5.30 eV for TFB and PFB, respectively, on the largest work function substrates, i.e. 5.10–5.15 eV and 5.0 eV for PEDOT–PSS and UV-ozone Au, respectively. In other words, a deviation from the simple Schottky–Mott limit is observed when the Fermi level of the electrode approaches the HOMO edge of the polymer. Similar deviations were observed for several polymers and high work function electrodes [40,121], and interpreted in terms of Fermi level pinning above the HOMO or below the LUMO, as the work function of the electrode approaches the polymer IE or EA, respectively. More will be said on this point in the next section.

An important issue is whether the photoemission measurements done at the surface of the 8–10 nm films provide an accurate picture of the energetics of the interface. If one assumes that the molecular levels are flat across the film, the HOMO and vacuum level positions measured at the surface of the film indeed represent those at the interface, and the hole injection barrier can be deduced directly from the HOMO position relative to E_F. If, on the other hand, "band bending" occurs near the interface, the energy difference measured at the free surface of the film must be corrected to obtain the real interface hole injection barrier. The seven cases of Figs. 16 and 17

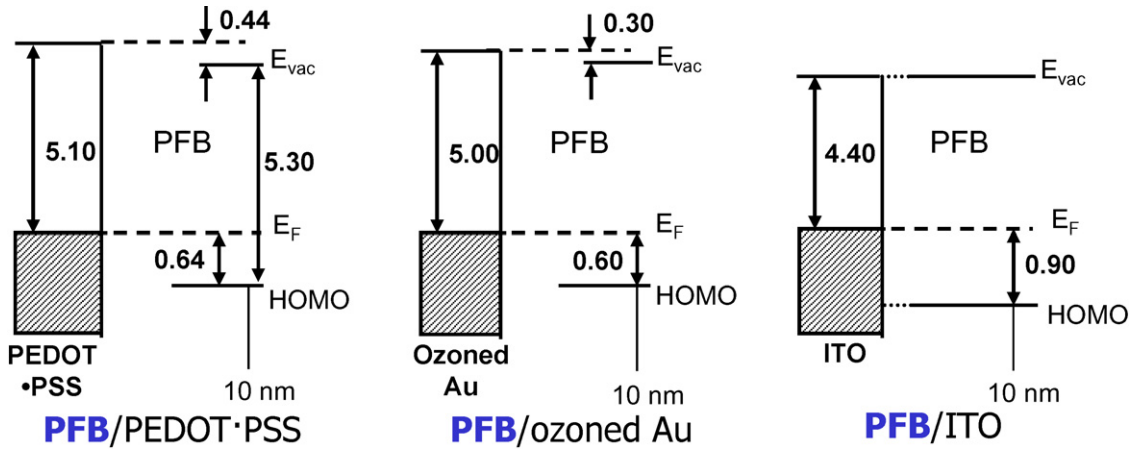

Fig. 17. Same as Fig. 16, for PFB (after [41]).

that follow the Schottky–Mott limit presumably correspond to flat band across the polymer film. In the three other cases, however, the shift in vacuum level could result from (i) an abrupt interface dipole followed by flat band across the film, or (ii) band bending into the film, followed by flat band across the film. Although the position of the HOMO with respect to E_F in the bulk of the material ultimately ends up being the same in both cases, the difference is more than academic. A (soft) band bending would correspond to a smaller hole barrier at the very interface than in the case of the abrupt dipole, leading to easier hole injection.

Further investigation of this point is done via UPS measurements on ultra-thin films prepared by spin-coating diluted polymer solutions, in order to probe the electronic structure of the material closer to the interface. The thickness of these films, estimated from concentration and spinning rates, was confirmed by AFM. The thinnest films realized here (~30 Å) show a significant density of pinholes (Fig. 18), but the coverage remains sufficient to extract valuable information on the molecular level energies. Films spun from more diluted solutions included a larger density of pinholes, but were not thinner. No gap states or additional interface-related features are detected via UPS near the interface, consistent with the absence of chemical interactions between polymer and substrate. A negligible shift of the HOMO level toward the Fermi level is observed for F8 with decreasing thickness, but the shift is consistently larger than 0.1 eV in the case of TFB. The extrapolation of an exponential fit to the data (Fig. 19) intersects the zero-thickness axis, i.e. the interface with the PEDOT–PSS substrate, around 0.35 eV on the E_F–HOMO edge scale. This is identical to the value resulting from vacuum level alignment between the polymer and the substrate, given the IE of TFB (5.5 eV) and the work function of PEDOT–PSS (5.15 eV). Similar experiments with ultra-thin TFB films on the lower work function substrates, i.e. Au (4.70 eV) and ITO (4.40 eV), show negligible band bending (Fig. 16), like for F8 on PEDOT–PSS, TFB on Au and on ITO.

According to these experiments, when a polymer film is deposited on a (relatively) low work function substrate that leads to a hole barrier larger than ~0.6 eV, flat band conditions prevail across the film, from interface to free surface (at least within the limits of the polymer thickness that can be investigated by photoelectron spectroscopy). On the other hand, when the polymer

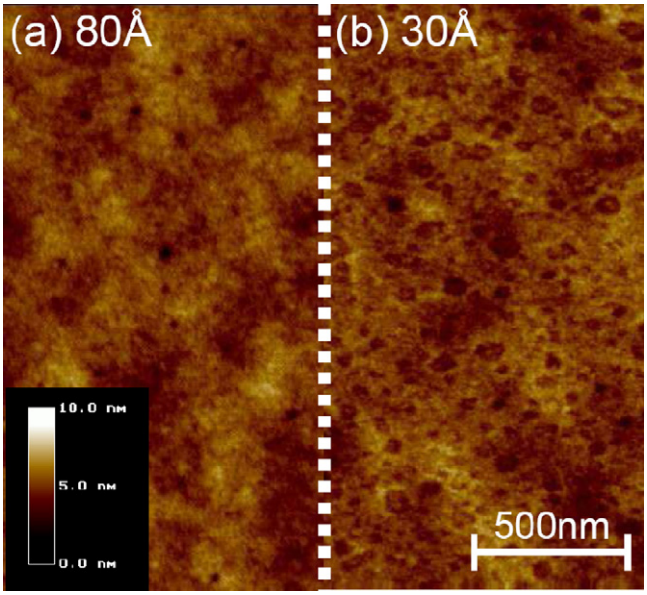

Fig. 18. AFM micrographs of (a) 80 Å TFB on PEDOT–PSS and (b) 30 Å TFB on PEDOT–PSS. In (b), the PEDOT–PSS substrate can be seen through pin holes in the TFB layer, with step size of ~30 Å (after [41]).

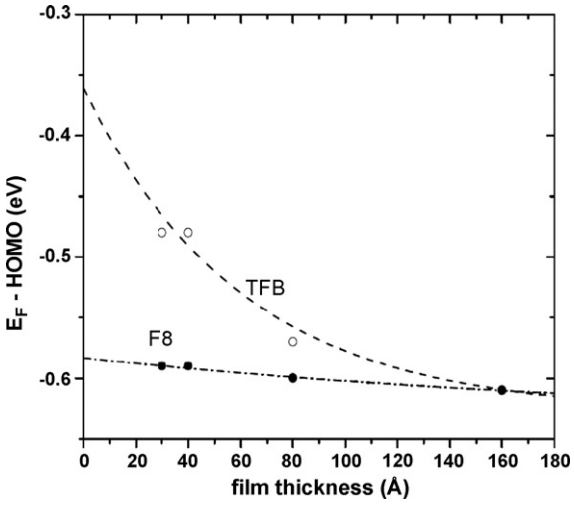

Fig. 19. Position of the HOMO edge obtained from UPS as a function of thickness of the polymer film deposited on a high work function electrode, e.g. PEDOT–PSS. F8 (●) exhibits near flat band across the film, while TFB (○) shows a shift at lower thickness, with an extrapolated intersection at 0.35 eV at zero thickness (after [41]).

film is spun on a high work function substrate, or by extension when the IE of the polymer is small, leading to a hole barrier of the order of 0.3–0.4 eV, the molecular levels undergo band bending away from their interfacial position and converge to a value corresponding to E_F–HOMO edge ~0.6 eV in the bulk of the material. This result is to be compared with results obtained on various polymers, including F8 (PFO) and TFB [40,121], interpreted in terms of Fermi level pinning leading to a minimum interface hole barrier of ~0.6 eV when the electrode Fermi level approaches the polymer HOMO edge. The discrepancy on the two interpretations is still under investigation, but could come from the fact that our measurements probe the interface on ultra-thin films, whereas other measurements may have been limited to the surface of a film with thickness of 80 Å and may not have been sensitive to the band bending away from the electrode interface.

While the experiments above focused predominantly on the hole-injection barrier, i.e. E_F–HOMO, and its limitations, recent work in our group also emphasized the electron-injection barrier in a polymer-on-electrode configuration. This is more unusual because, as mentioned above, the electron-injector is generally a low work function metal like Al or Ca evaporated on the polymer. However, recent work by Liu et al. [122] demonstrated the very interesting possibility of using lamination to physically join two separately prepared parts of a PLED to make a fully operational and efficient device. In such a context, the formation of the electron-injection contact by spin-coating the polymer on the cathode makes good sense. In the example presented below, the cathode is an aluminum film covered by a native oxide (AlOx), and modified with a self-assembled monolayer (SAM) of octylphosphonic acid (Fig. 20a) [33]. UPS measurements of the AlOx substrate, without and with SAM, and of the polymer film spun on top of this substrate, are shown in Fig. 20b. The work function of the unmodified AlOx surface is 3.8 eV, ~0.4 eV smaller than that of the clean Al surface, leading to an electron injection barrier, i.e. LUMO edge–E_F, of 1.14 eV (Fig. 20c). The work function of the SAM-modified AlOx surface is reduced to 3.3 eV by the interface dipole arising between the phosphonate molecule and the oxide, leading to an electron injection barrier of 0.72 eV. An increase of two orders of magnitude in electron injection (not shown here) results from this electrode modification and from the corresponding barrier lowering [33]. Interestingly, exposure of the SAM-modified AlOx to X-rays during XPS analysis reduces the electrode work function by another 0.3 eV, down to 3.03 eV (via a mechanism that is not

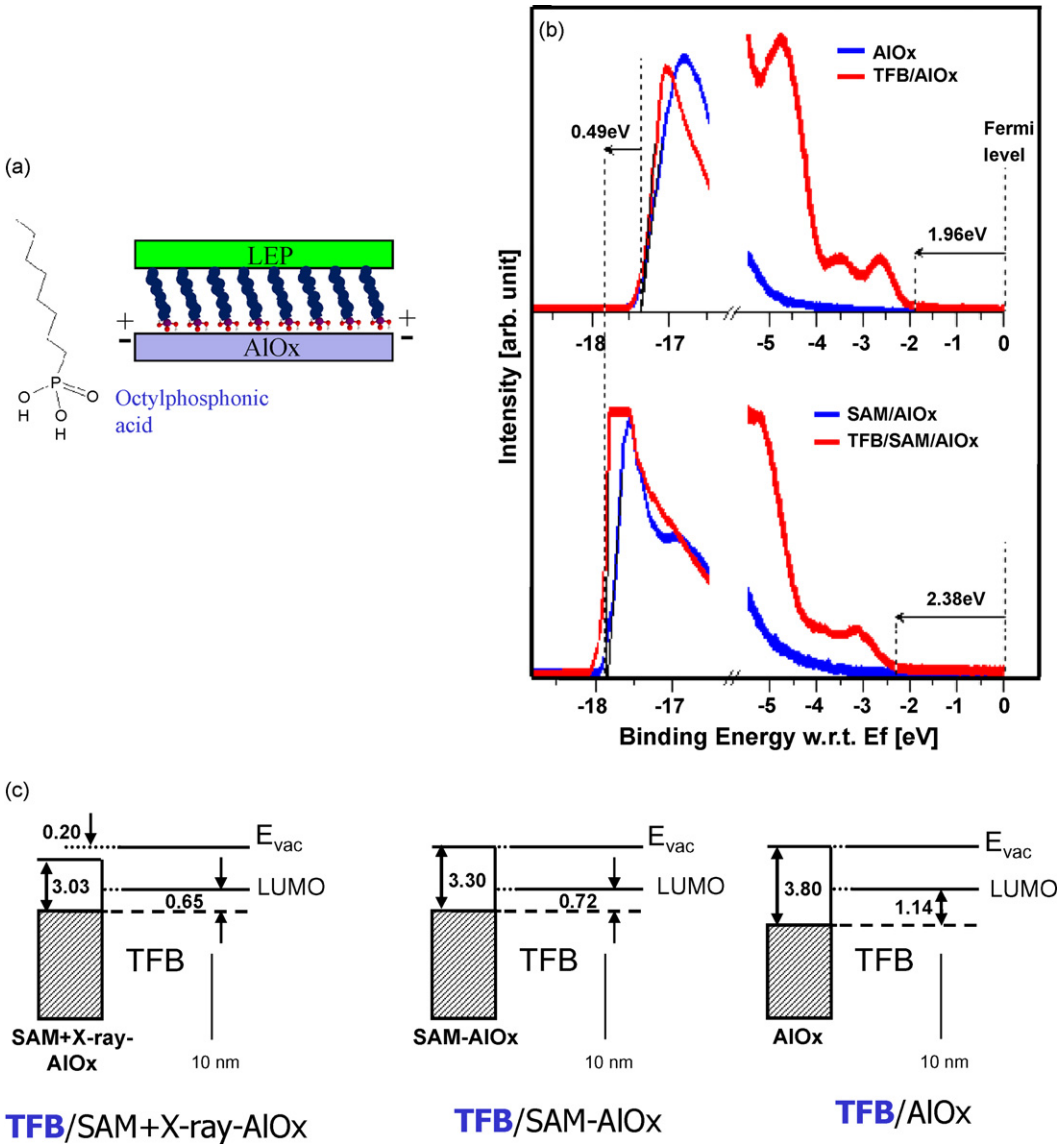

Fig. 20. (a) Schematic of the TFB film/octylphosphonate SAM/AlOx substrate; (b) He I spectra of the AlOx (blue) and polymer film (red), without (top) and with (bottom) the SAM; the 0.49 eV shift of the photoemission onset around 17–18 eV indicates the SAM-induced decrease of the AlOx work function; (c) energy positions of the vacuum level and LUMO level of TFB measured at the surface of a 10 nm thick polymer film spin-coated on as loaded AlOx, SAM-modified AlOx, and SAM-modified AlOx following X-ray exposure. The substrate work function, E_F and bulk LUMO–E_F are indicated in each case. (For interpretation of the references to color in this figure legend, the reader is referred to the web version of the article.)

understood at this point), yet the Fermi level approaches the LUMO by only 70 meV and an interface dipole develops at the polymer–electrode interface [123]. This smaller than expected shift and the interface dipole indicates partial pinning of E_F as it approaches the polymer LUMO, as was observed and outlined above for E_F approaching the HOMO. Note that the Fermi level position was measured here only at the surface of the 10 nm polymer film. Thinner films were not investigated to evaluate eventual interface band bending, like in Fig. 19.

In summary, while it is obvious from simple consideration of charge balance at metal–semiconductor interfaces that pinning of the Fermi level should occur when the electrode work function is equal to, or larger (smaller) than, the organic semiconductor IE (EA), the experiments demonstrate that E_F does not approach the band edge closer than ~0.6 eV in the bulk of polymer films investigated here, or those investigated by Tengstedt et al. [40] and Fahlman et al. [121]. The interface barrier may be somewhat smaller (~0.35 eV), but in that case is accompanied by band bending that moves E_F back to the 0.6 eV limit in the bulk of the film. For an electrode work function well within the organic gap, i.e. $EA + \delta < WF < IE - \delta$ with $\delta \sim 0.6$ eV, the interface barrier obeys the Schottky–Mott limit, as already depicted in Fig. 3.

4.3. Pinning of the Fermi level: polaron state vs. tail gap states

Pinning of E_F when the electrode work function approaches the organic IE or EA is an important phenomenon that affects charge injection and should be taken into consideration when designing contacts. The phenomenon has been recently explained using two different models: the Integer Charge Transfer (ICT) model [121], and E_F pinning in the tail of the polymer gap states [41].

The ICT model proposes that, as the Fermi level of the electrode approaches the edge of the gap with increasing or decreasing work function, it eventually comes to the level of the interface polaron (positive polaron in the bottom part of the gap, and negative polaron in the upper part of the gap). The interface polaron can be thought of as the bulk polaron stabilized by the extra polarization from the electrode, and thus is expected to be slightly deeper in the

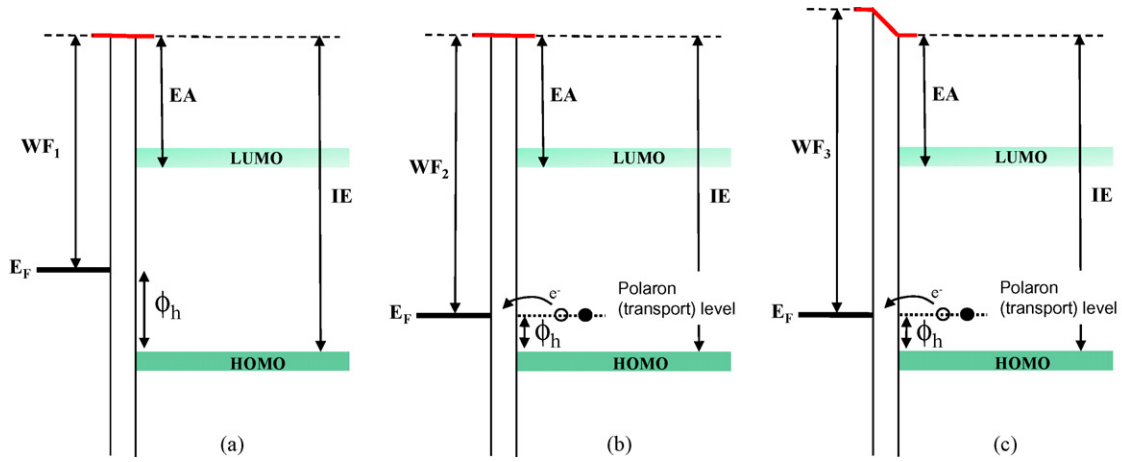

Fig. 21. Schematic of a polymer/electrode interface energetics according to the ICT model. (a) With moderate work function WF_1, the interface E_F is deep in the gap. (b) As the electrode work function increases ($WF_1 < WF_2$), the interface E_F approaches the HOMO until it reaches the polaron level. (c) A larger work function ($WF_2 < WF_3$) leads to E_F pinning, charge transfer and formation of an interface dipole.

gap than its bulk counterpart. As the electrode E_F reaches this level, charge is transferred to the polaron state, an interface dipole is formed, and the Fermi level is pinned (Fig. 21). The model assumes that the pinning position is significantly detached, i.e. by ~0.6 eV, from the edge of occupied and unoccupied states measured by UPS or IPES because of the relaxation energy of the molecule or polymer chain occupied by a charge, energy that is not included in the spectroscopy because of the time scale of intra-molecular nuclear motion (see Section 3) [85]. It is the opinion of the authors of the present review that the relaxation energy quoted for this process is excessive and should be of the order of 0.2 eV, significantly smaller than the difference between E_F pinning position and edge of the HOMO or LUMO measured via spectroscopy.

Hwang et al. [41] proposed a model based on the broadening of the density of states in molecular and polymer materials and the subsequent E_F pinning in the tail of these states. The tailing of the DOS in the gap of the material, briefly discussed at the end of Section 4.1.2, was experimentally investigated for PPV by Hulea et al. [116] using an electrochemically gated transistor, and for *N*;*N*^{I}-diphenyl-*N*,*N*^{I}-bis(1-naphthyl)-1,10-biphenyl–4,4^{II}-diamine (α-NPD) by Tal et al. [117] using a Kelvin probe force microscope on an OFET structure. Both methods on both materials showed that (i) the shape of the DOS is quite complex, and (ii) the shape can be approximated with a combination of a Gaussian in the high DOS region (closer the HOMO) and an exponential tail in the lower DOS region. Celebi et al. interpret similar Kelvin probe measurements on CuPc with a single exponential dependence of the DOS [118]. The former two investigations, however, suggest the presence of a significant DOS at about 0.7 eV from the *center* of the molecular state, or about 0.2–0.3 eV from the edge measured by UPS (or IPES). Adding to that number a more realistic 0.2 eV for the relaxation energy of the charge molecular ion (not seen in spectroscopy), one can reasonably justify pinning of the Fermi level at a position of 0.4–0.5 eV away from the "band edge", as indeed observed experimentally for the polymer films investigated here. This energy difference is generally observed to be smaller, i.e. 0.3 eV, for small molecule films, presumably because of smaller static disorder broadening of the DOS.

This model of E_F pinning in the tail of gap states broadened by disorder is indirectly supported by the fact that smaller E_F–HOMO values equal to 0.2–0.3 eV have been found for other systems, like poly-(3-hexylthiophene) (P3HT) in contact with PEDOT:PSS [124]), which are known to form more crystalline structures in thin films.

Pinning of the Fermi level also suggests an explanation for the "band bending" mentioned in the previous section for interfaces between high work function electrodes and small (or medium) ionization energy polymers (Fig. 19). As E_F approaches the frontier orbitals of the polymer at the interface, the tail of the density of states extending into the gap fills up, and an excess density of charges accumulates in the organic material (holes, in the case of electrodes with work function close to the polymer IE). These interface charges induce an electric field that displaces the frontier orbital, e.g. the HOMO level, away from E_F [125] to limit further penetration of charges into the bulk of the film (Fig. 22b). The density of excess interface holes depends on the barrier. When the barrier is smaller or equal to 0.4 eV, this density is sufficient to bend the bands by 0.2–0.3 eV within the thickness measured by UPS (<200 Å). On the other hand, when the hole barrier is equal to or larger than 0.6 eV, the charge density is small and the field does not induce a significant band bending over the range of thickness investigated here (Fig. 22a).

4.4. Energy level alignment at metal-on-polymer interfaces

Injection barriers at the top contact interface (metal-on-polymer) are more difficult to determine than those at the bottom contact interface (polymer-on-metal). UPS measurements are used, as described above, to determine the energy difference between the metal E_F and the polymer frontier orbital, i.e. the injection barrier. However, the signal from the incrementally deposited metal overlayer rapidly masks that of the polymer [96], hindering the determination of the edge of the frontier orbital of the organic material, and making the determination of the barrier under formation more difficult. Unlike their polymer-on-metal counterparts, metal-on-polymer interfaces are also often diffuse. They exhibit various metal growth modes, depending on the metal, which makes the analysis more complicated. A combination of UPS, XPS and injection *I*–*V* measurements are presented here to approach these interfaces.

For interface energetics and chemistry measurements, the metals were typically deposited on ~200 Å thick polymer films, i.e. thick enough to eliminate any interference from the substrate and thin enough to prevent charging upon photoemission spectroscopy. Thicker films (500–1000 Å) were used for *I*–*V* measurements. Thermal evaporators were used for aluminum (Al), samarium (Sm) and gold (Au), and an electron-beam evaporator was used for silver (Ag) and platinum (Pt). Layer-by-layer metal growth experiments were performed with deposition rates ranging between 0.01 Å/s and 0.05 Å/s, whereas thick films for top device contacts were deposited at rates between 0.1 Å/s and

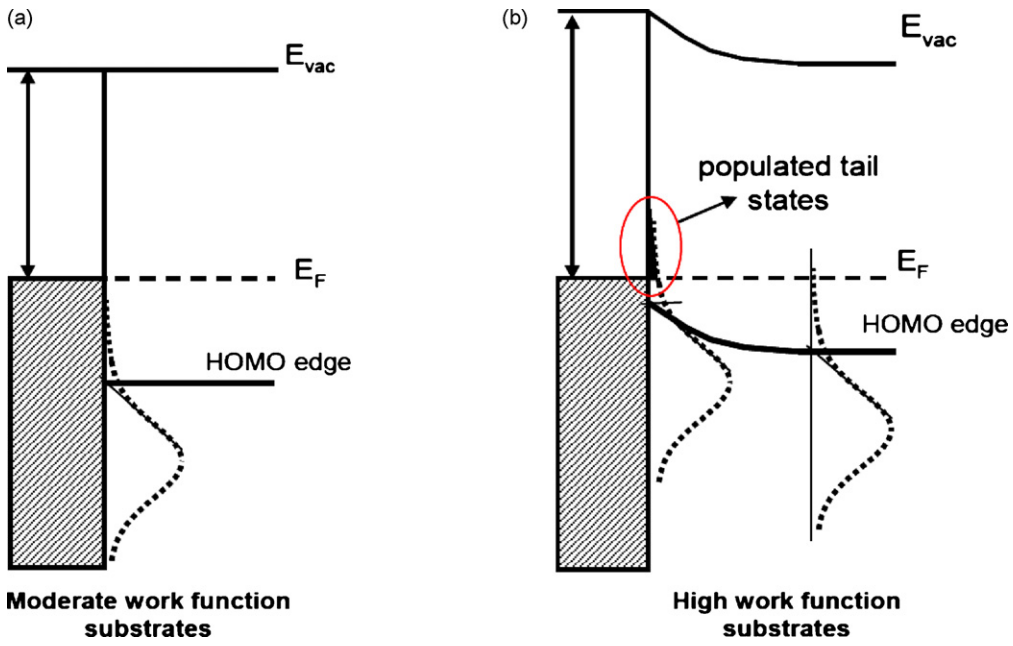

Fig. 22. Schematic diagrams of energy band alignment and charge population profile in Gaussian shaped density of states of polymer in contact with (a) moderate work function material and (b) high work function material. The tail states are populated with holes at the interface when the polymer is in contact with a high work function material (after [104]).

0.15 Å/s. All depositions were performed in UHV, at pressures below 5×10^{-9} Torr, insuring ultra-clean metal films and interfaces (verified via XPS and Auger electron spectroscopy).

We give below the full analysis of the formation of one metal-on-polymer interface, i.e. Al-on-TFB. The results obtained for the other metals are summarized in the following sections.

4.4.1. Al on TFB and F8

UPS and XPS spectra recorded for different thicknesses of Al deposited on TFB are shown in Fig. 23. In the UPS spectra, the TFB features remain visible up to a nominal thickness of 50 Å of Al, with only small change in the shape and relative valence peak positions. The slow decrease of the TFB features indicates that the polymer surface is not fully covered by Al, even at high coverage (20–50 Å). Furthermore, the line-shape of the UPS spectrum, and thus the electronic structure of the material, does not appear to be significantly affected by the Al deposition, indicating minimal chemical interaction. XPS shows that the width (σ) of the C 1s core level increases by only ~0.05 eV, a feature that may be due to the metal-induced band bending near the polymer surface but is not attributed to chemistry. Finally, the Al 2p core level shows no additional "reacted" component to the metallic Al peak at ~72.8 eV. These observations lead to the conclusion that Al forms islands upon deposition on TFB, without inducing significant chemical reaction. The work function of the film, the binding energy of the HOMO and C 1s core level, and the intensity of C 1s peak are shown in Fig. 24 as a function of the nominal thickness of deposited Al [104]. After deposition of 20 Å Al, the work function converges to ~4.1 eV, a value close to the canonical work function of metal Al. The work function of the film and the position of the HOMO evolve in a parallel fashion (Fig. 24a), indicating that the IE of TFB remains basically constant throughout the deposition, and suggesting that the TFB remains intact. Yet, the evolution of the C1s binding energy is different from that of the TFB HOMO and of the

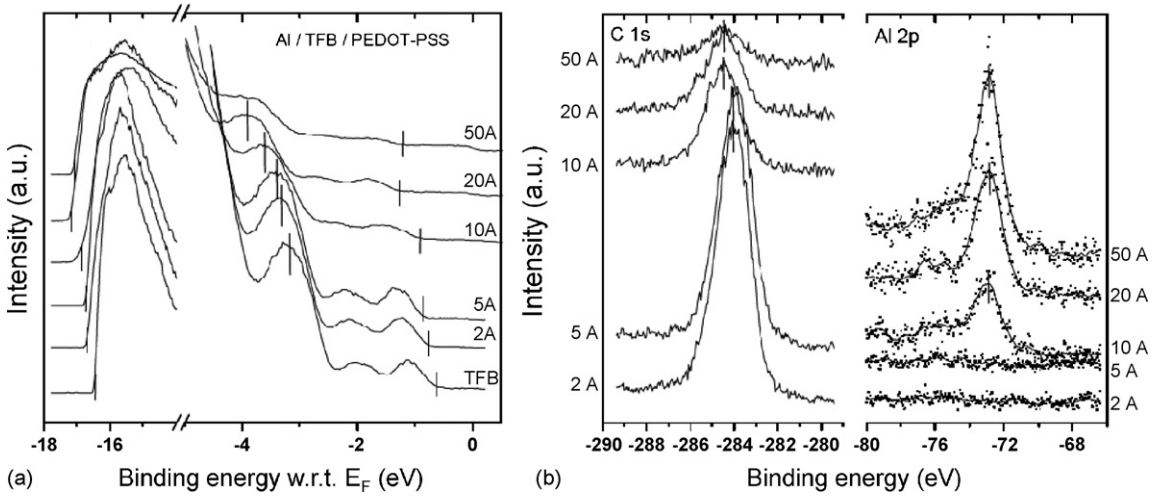

Fig. 23. (a) UPS and (b) XPS spectra measured for 0, 2, 5, 10, 20, and 50 Å of Al deposited on TFB (after [77]).

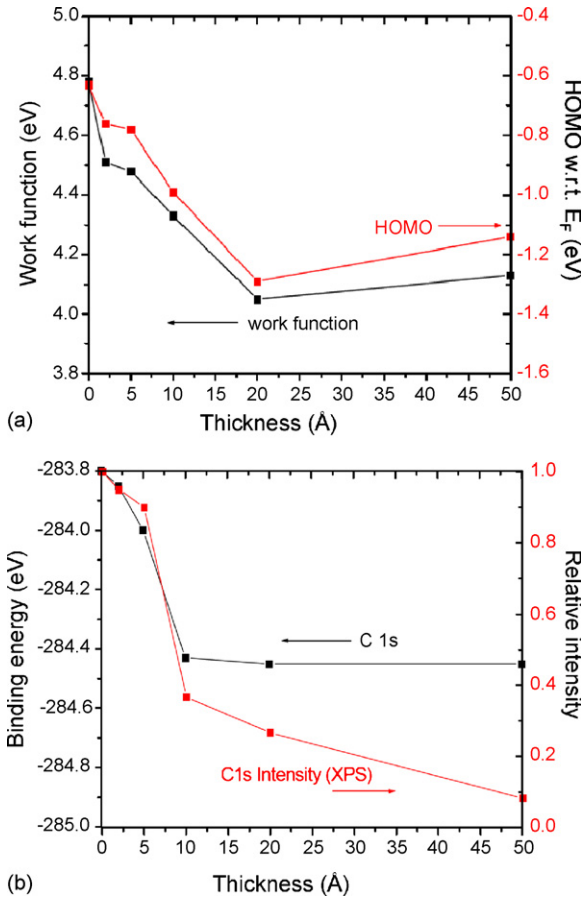

Fig. 24. (a) Work function and HOMO position w.r.t. E_F, and (b) position of the C 1s core level and its intensity, as a function of Al deposition on TFB (after [104]).

film work function at thickness of 5 and 10 Å (Fig. 24b). This can be understood when the position of the Al Fermi step is carefully analyzed (data not shown here). The position of the Fermi step, which should be constant and aligned with the Fermi level of the system throughout the measurement, is actually found at 0.3 eV higher binding energy. This type of behavior is indicative of a non-equilibrium situation due either to photon-irradiation-induced surface photovoltage (SPV) or charging. In SPV, light generates electron–hole pairs, and the minority carriers in a semiconductor with band bending/tilting, accumulate at the surface/interface, and induce an electric field that tends to flatten the bands [126–129]. Here, the energy alignment at the interface between TFB and the substrate is fixed, but the potential at the TFB surface changes even with low Al coverage, leading to a tilt in the energy band across the device structure (Fig. 25a). UV illumination (in UPS) generates SPV or charging, and thus the shift of the Al Fermi step. As the thickness of Al increases and Al forms a complete metallic layer, the photo-generated charges can easily recombine in the Al layer, and the effect disappears. In XPS, however, the photon flux is significantly smaller than in UPS, and SPV or charging is negligible. By shifting the 10 Å Al UPS spectrum by 0.3 eV, we find that the evolution of the positions of the various photoemission onsets, HOMO, and C 1s core level as a function of Al deposition agree precisely with each other. The TFB HOMO position following Al deposition and the corresponding hole injection barrier can therefore be deduced from the initial position with respect to E_F (bottom spectrum in Fig. 23a) [77] shifted by the Al-induced C1s core level shift (Figs. 23b and 24b).

In summary, Al vacuum-evaporated on TFB forms an interface that closely follows vacuum level alignment. The hole injection barrier (E_F–HOMO) is ~1.35 eV (Fig. 25a) and the electron injection barrier (LUMO–E_F) is equal to the transport gap (E_t) minus the hole barrier, i.e. 3.25 − 1.35 = 1.90 eV (we provide here the electron barrier, as Al is generally used as an electron injection contact). The interface displays no obvious signs of chemical reaction, and the Al tends to form island upon deposition without any evidence of interdiffusion. A similar behavior is found for Al on F8, and the interface energetics correspond to a hole (electron) injection barrier of ~1.60 eV (1.90 eV).

4.4.2. Ag and Sm on TFB and F8

The same type of analysis applied to these four interfaces leads to the following general conclusions. Ag forms non-reactive interfaces with both polymers, initially grows in three-dimensional clusters, and leads to holes injection barriers equal to ~1.65 eV and ~1.70 eV on TFB and F8, respectively. Interestingly, these barriers are 0.1–0.2 eV *larger* than those produced by Al, although the work function of Ag generally expected to be ~0.1 eV *larger* than that of Al. Some indications of an interface dipole are also obtained, although a precise determination of this aspect of the interface is clearly difficult. The interface energetics for Ag on F8 are summarized in Fig. 25b.

In contrast to Al and Ag, Sm (work function = 2.7 eV) wets the surface and forms a two-dimensional film on both polymers even in the early stages of deposition, leading to an exponential decrease of the polymer photoemission features as a function of Sm thickness. This behavior is consistent with a chemical interaction with the polymer, as confirmed by a significant broadening of the C 1s core level feature. Decomposition of the latter suggests that the chemical interaction is limited to the top 1–2 molecular layers of the polymer film only, allowing a relatively safe evaluation of the Sm-induced molecular shifts through the shift of the bulk C 1s core level. The analysis yields E_F–HOMO = 2.2 eV, giving an electron injection barrier of 0.9 eV with a 0.5–0.6 eV dipole barrier for Sm on TFB (Fig. 25c). The corresponding numbers for Sm on F8 are 2.4 eV and 1.1 eV, respectively.

4.4.3. Two noble metals on TFB and F8

As in the case of Sm, the exponential decay of the polymer C1s upon Pt deposition suggests a layer-by-layer growth, although chemical reaction at the interface cannot be ruled out. The width of the C 1s peak increases by ~0.15 eV with Pt deposition, significantly smaller than in the Sm case, but larger than in the Al and Ag cases. The determination of the interface alignment of molecular levels is complicated by the rapid decay of the valence molecular features vs. Pt coverage in UPS. The analysis is based here not on the bulk C 1s core level shift, which becomes unreliable in view of possible Pt-molecule reaction, but on the measurement of injected charges to infer the hole injection barrier at the top contact. *I–V* measurements performed on a Pt/TFB/Pt simple diode are shown in Fig. 5. The two curves correspond to the hole current injected from the bottom Pt, i.e. polymer-on-Pt, and the top Pt, Pt-on-polymer. Given the high work function of Pt (~5.5 eV clean and ~5.1 eV contaminated), the electron barrier at both bottom and top interfaces is expected to be large, and the current measured with both polarities is essentially a single carrier hole current. This is consistent with the fact that no electroluminescence is observed, even at high bias across the device during the *I–V* measurement. Surprisingly, the hole current injected from the top Pt contact is four to five orders of magnitude smaller than that from the bottom Pt contact. Assuming a simple injection-limited current in both cases, this translates into a 0.3–0.4 eV larger hole barrier for the top contact. With the TFB-on-Pt hole barrier measured at 0.5 eV, the top Pt hole barrier is estimated at ~0.9 ± 0.1 eV. The energetics of these two TFB interfaces are summarized in Fig. 25d. Similar results (asymmetric injection) have been reported for small molecule

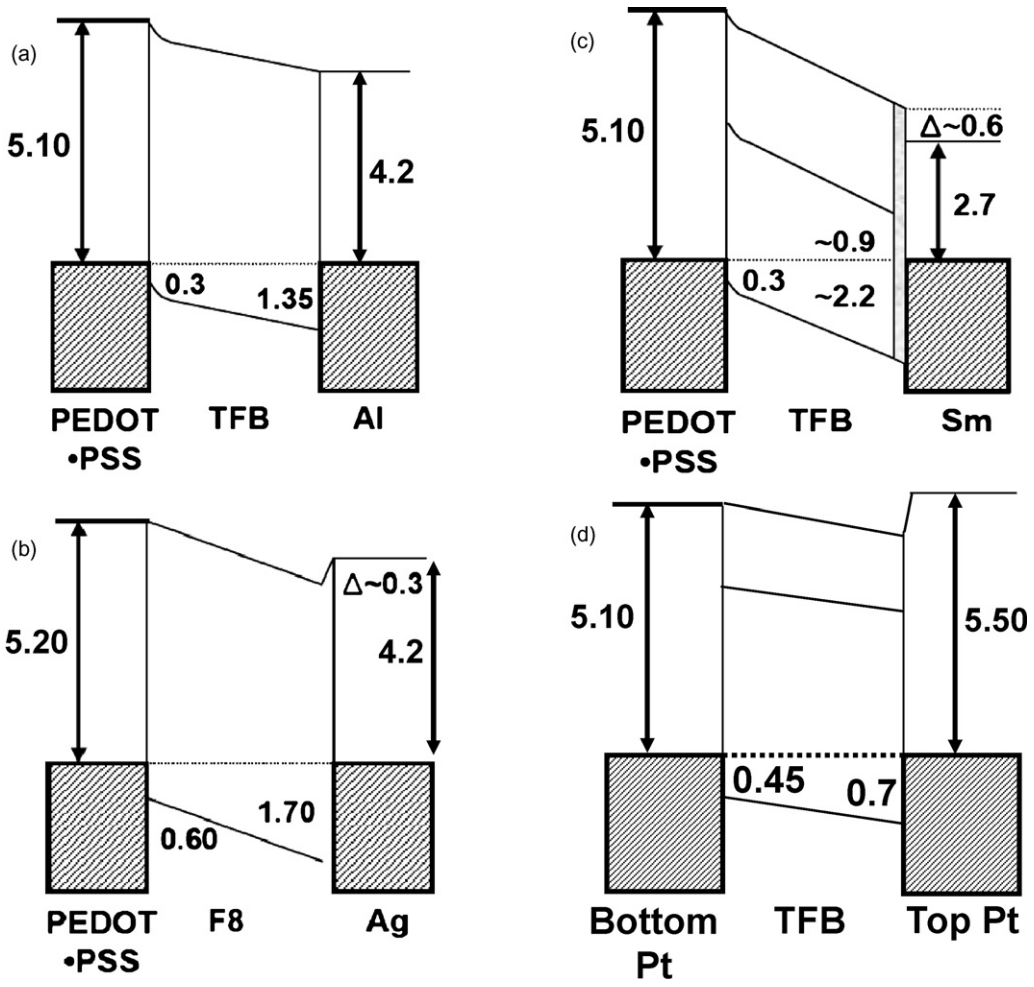

Fig. 25. Energetics of sandwich structures formed by spin-coating the polymer on the left electrode and vacuum evaporation of the right electrode: (a) PEDOT–PSS/TFB/Al; (b) PEDOT–PSS/F8/Ag; (c) PEDOT–PSS/TFB/Sm; and (d) Pt/TFB/Pt (after [104]).

devices, when the substrate (bottom contact) is exposed to air prior to organic deposition (Section 5). Chemical reaction and difference in interface morphology cannot be ruled out in the explanation of the difference between the bottom and top Pt contacts to F8 and TFB. Yet, the remainder of this review shows that this type of asymmetry in injection is a very general phenomenon for polymer and small molecule films alike, the origin of which can be traced in the significant difference in interaction between the organic film and the clean or contaminated electrode.

Lastly, Au brings another issue for the top vacuum-deposited contact, namely that of interdiffusion and formation of traps in the bulk of the polymer. The UPS polymer features disappear with the deposition of ~10 Å of Au, however, the complete elimination of the C1s peak intensity in XPS requires more than 300 Å of Au. This is consistent with interdiffusion of the metal, with significant distortion of the electronic structure of the permeated polymer layers. *I–V* measurements performed on a simple diode structure with evaporated Au top contact confirm this interpretation. The hole current measured in the dark decreases after each scan. However, this degradation is not permanent, and the current can be restored to its initial value by a flash of white light on the sample. When the same sample is measured under light, no change in current is observed. This behavior is typically observed in a structure with traps embedded in the semiconductor. In contrast, the current in the device with Pt top contact remains stable over many scans. Since the only difference between the two metal contacts is the morphology of the metal film during the initial sequences of deposition, the conclusion is that the hole traps are induced by Au diffusion and formation of nano-clusters [130,131].

4.5. Discussion on interface energetics of top vs. bottom contacts

A summary of energy levels and Fermi level positions in the energy gap of F8 and TFB for bottom (polymer spun on electrode) and top (mostly top evaporated metal) contacts with various substrates electrodes (from the above sections) is shown in Fig. 26. With the transport gaps measured with UPS/IPES, the figure serve as a reference for hole and electron injection barriers at interfaces between these two polymers and the materials studied in this work. These data are re-plotted in Fig. 27, which shows the dependence of the (hole) barrier, i.e. E_F–HOMO edge, on the work function of the material in contact for both polymer-on-electrodes and electrodes-on-polymer. The rate of change of the barrier vs. the electrode work function is described by the slope parameter (S), i.e. a measured of the screening of the semiconductor polymer/electrode interaction at the interface. Note that the electrode work function, in the case of bottom contacts, is measured with UPS *after* exposing the surface to the solvent to simulate the polymer spin coating process. On the other hand, the work function of the top electrode is assumed to be similar to that of a freshly evaporated, atomically clean film of this material. The validity of the assumption has been proven in various chemically non-interacting metal–small molecule systems, where the injection barrier at top

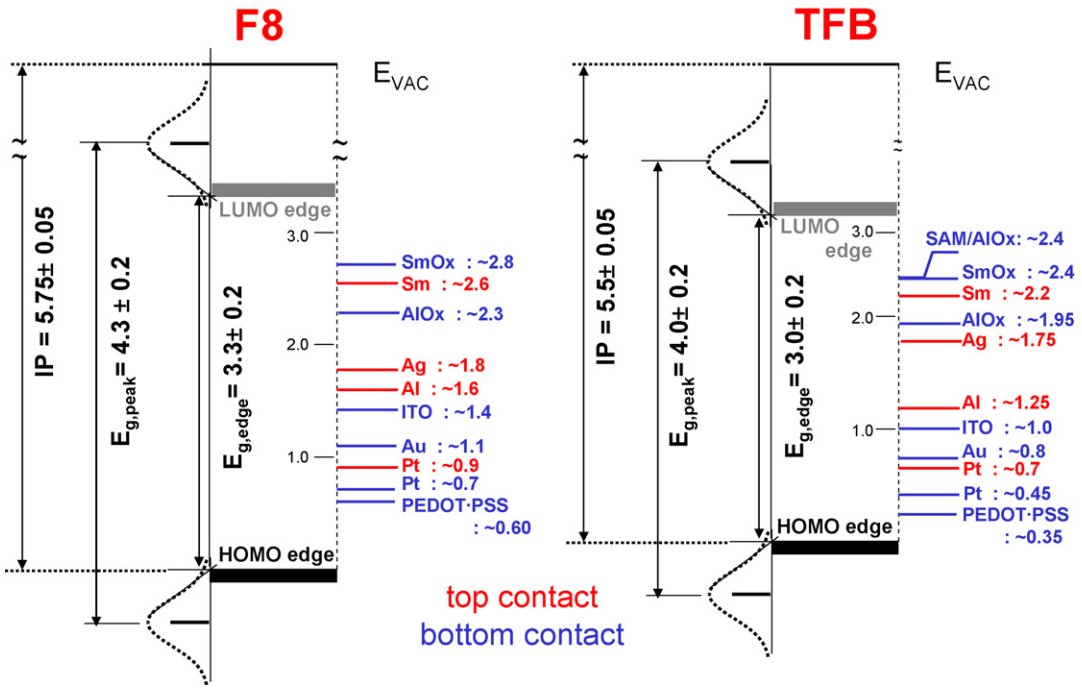

Fig. 26. Key energy levels and E_F position in the gap of F8 and TFB at interfaces with various substrates and metals. E_F positions corresponding to polymer-on-substrate interfaces (metal-on-polymer interfaces) are marked in blue (red). Energies denote the corresponding hole-injection barriers, i.e. E_F–HOMO (after [104]). (For interpretation of the references to color in this figure legend, the reader is referred to the web version of the article.)

and bottom contact is the same when both contacts are freshly evaporated in UHV [49,75,132].

As discussed in previous sections and shown in Figs. 3 and 27, the interface energetics of the bottom contacts are predominantly governed by vacuum level alignment, with $S = 1$, provided that the electrode work function remains smaller and larger by 0.3–0.5 eV than the polymer IE and EA, respectively. The substrates are usually prepared in air or nitrogen atmosphere, and the polymer is spun in nitrogen atmosphere from a solvent solution. The polymer/substrate interface can be characterized as "contaminated". The contaminants (hydrocarbons in air, residual solvent molecules) can be thought of as passivating the electrode surface, decreasing the chemical interaction (chemistry and bonding) between the two materials. In the framework of the induced density of interface state (IDIS) model, this layer physically and electronically decouples the organic film from the continuum of the metallic electronic states [44]. This in turns, reduces the density of interface states induced in the gap of the organic material, reduces the interface dipole and in the extreme cases described here, results in vacuum-level alignment.

In contrast, the hole barriers obtained at the top contact fall on a different line with $S = 0.55 \pm 0.05$, suggesting a different mechanism for energy alignment. The top contact is processed in vacuum and the "contaminants" that were present in the spin coating case are absent. The mode of deposition also leads to a more "intimate" contact, with the metal forming stronger bonds and penetrating to various degrees in the polymer film. Therefore, a larger density of metal valence states overlaps with the gap of the polymer, resulting in a stronger

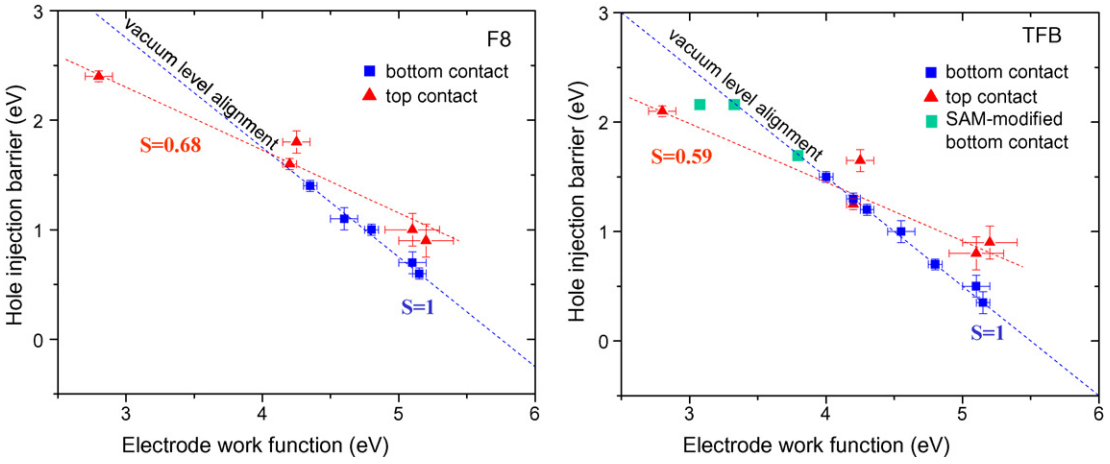

Fig. 27. Interface E_F–HOMO vs. electrode work function in (a) F8 and (b) TFB for top evaporated electrode (red triangles), bottom electrode (blue squares) and AlOx and SAM-modified AlOx bottom electrode (green squares). The data points for the bottom contacts fall on the vacuum level alignment line ($S = 1$), while the data points for the top contact follow a linear dependence with $S < 1$. (For interpretation of the references to color in this figure legend, the reader is referred to the web version of the article.)

interaction, stronger "pinning" of the Fermi level in the energy gap and, generally, a larger interface dipole. Similar results can be found in small molecule systems, as will be described in the next section. The energy alignment at the interface between small molecules and metals generally departs from the Schottky–Mott limit and has been explained with several different models (Section 2.1.2). The results presented here therefore suggest that polymer interfaces are not fundamentally different from small molecule interfaces, but that the inevitable contamination resulting from solution processing environment leads to the canonical Schottky–Mott limit generally assumed for polymer interfaces.

5. Energetics of small molecule–electrode interfaces

Much has been written on this topic in the past decade, and detailed reviews of general results and interpretations have already been published [45,46,49,72,133–135]. The purpose of this section is not therefore to review the considerable body of work published on small molecule film interfaces, but rather to focus on the specific issue of the differences between the energetics of molecules-on-electrode and electrode-on-molecules, with and without interface contamination. The IE and EA of films of small molecules used in this review are given in Table 1, and more graphically in Figs. 7 and 8.

The solution-based processing of polymer-on-electrode interfaces necessarily limits investigations of the mechanisms that control interface energetics because of the initial (chemical, electronic) state of the electrode. On the other hand, the ability to vacuum-deposit small molecules on controllably prepared electrode surfaces, i.e. from atomically clean metal surfaces to surfaces controllably exposed to a specific atmosphere, provides sufficient flexibility in interface formation to answer basic questions on the impact of the processing sequence and environmental conditions on the charge injection barriers. Once these issues have been explored, a direct comparison between small molecule and polymer interfaces becomes possible.

5.1. Molecule-on-metal vs. metal-on-molecule interfaces

Organic materials, in particular small molecule films, are soft materials bound by weak intermolecular vdW-type bonds. It is therefore expected that metal-on-organic interfaces will be morphologically different from their organic-on-metal counterparts. When organic molecules are vacuum-evaporated on a metal surface, the interface is expected to be abrupt (Fig. 28). Chemical reaction may take place at the first molecular layer in contact with the metal, but negligible interdiffusion should result across the interface. On the other hand, the commonly accepted picture of "small" metal atoms vacuum-evaporated, i.e. carrying significant thermal energy, and impinging on a soft and relatively open organic matrix is one where chemical reaction and interdiffusion can occur relatively deep in the organic film (Fig. 28). Experimental evidence, examined above for polymers, is given in Fig. 29 with XPS data recorded for the Alq_3–Mg system. Panel (a) shows the attenuation of the Mg 2p core level as a function of Alq_3 deposition on a Mg film, and panel (b) shows the attenuation of the Alq_3 C 1s core level as a function of Mg coverage for the reverse deposition sequence [75]. From the rates of attenuation of these two core levels, it is clear that the Alq_3 film grows two-dimensionally on the metal surface, whereas the Mg film covers the organic surface very slowly. Additionally, panel (c) shows that most of the Mg is oxidized in the initial stages of the deposition on Alq_3 and reaches metallicity only after deposition of 30–60 Å, a clear indication of diffusion into, and/or chemical reaction with, the host film, rather than a simple surface clustering. Although both interfaces show evidence of chemical reaction, the Mg-on-Alq_3 interface is marked by extensive interdiffusion, whereas the Alq_3-on-Mg interface is abrupt.

An important question is whether the difference in interface morphology necessarily implies a difference in electrical behavior, in particular with regard to charge injection. The *I–V* characteristics taken from metal/Alq_3/metal sandwiches (metal = Mg, Al, Sm) built in UHV using atomically clean bottom metal contacts, shown in Figs. 5 and 30, partially answer this question. The symmetry in current vs. bias direction over 5–6 orders of magnitude of the electron currents injected from top and bottom contacts clearly demonstrates electrical equivalence of the abrupt and diffused interfaces. Note that early measurements on Mg:Ag/Alq_3/Mg:Ag structures showed a top-injected electron current 2–3 orders of magnitude *larger* than the bottom-injected electron current [136]. The difference was attributed to gap states induced in the organic material by (top contact) metal deposition, which created intermediate states between the metal Fermi level and the LUMO of the organics. This result was later reversed [132] by the demonstration that the effect was due to contamination of the reactive Mg bottom electrode in the low-vacuum system used for these experiments, and that all-UHV processing insured symmetry of interface energetics and injection. A situation similar to that of Alq_3 structures made in UHV is also observed for Au/α-NPD/Au

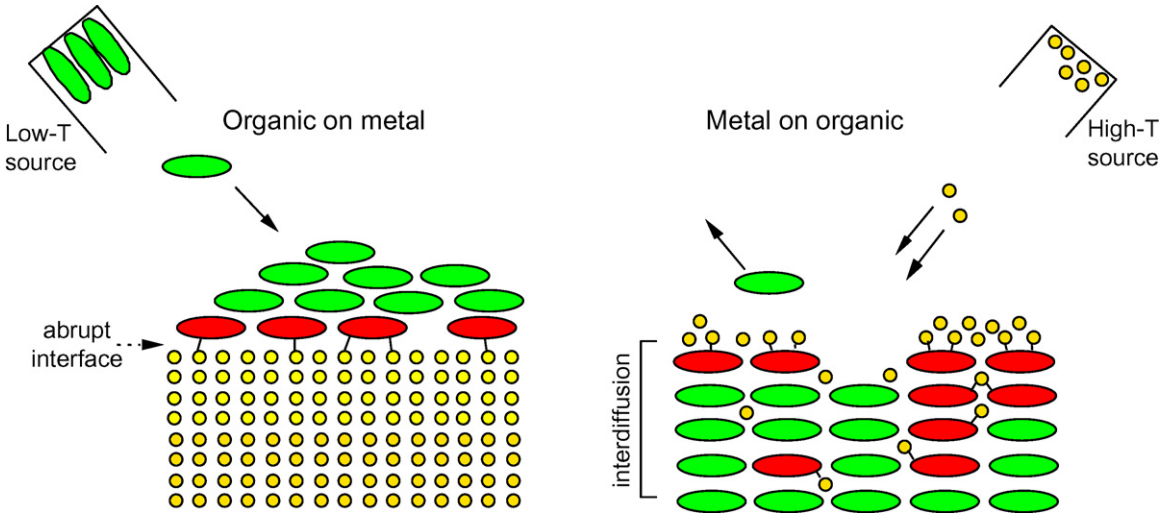

Fig. 28. Conceptual view of interfaces corresponding to small molecules vacuum-deposited on a metal surface vs. metal atoms vacuum-evaporated on a small molecule film.

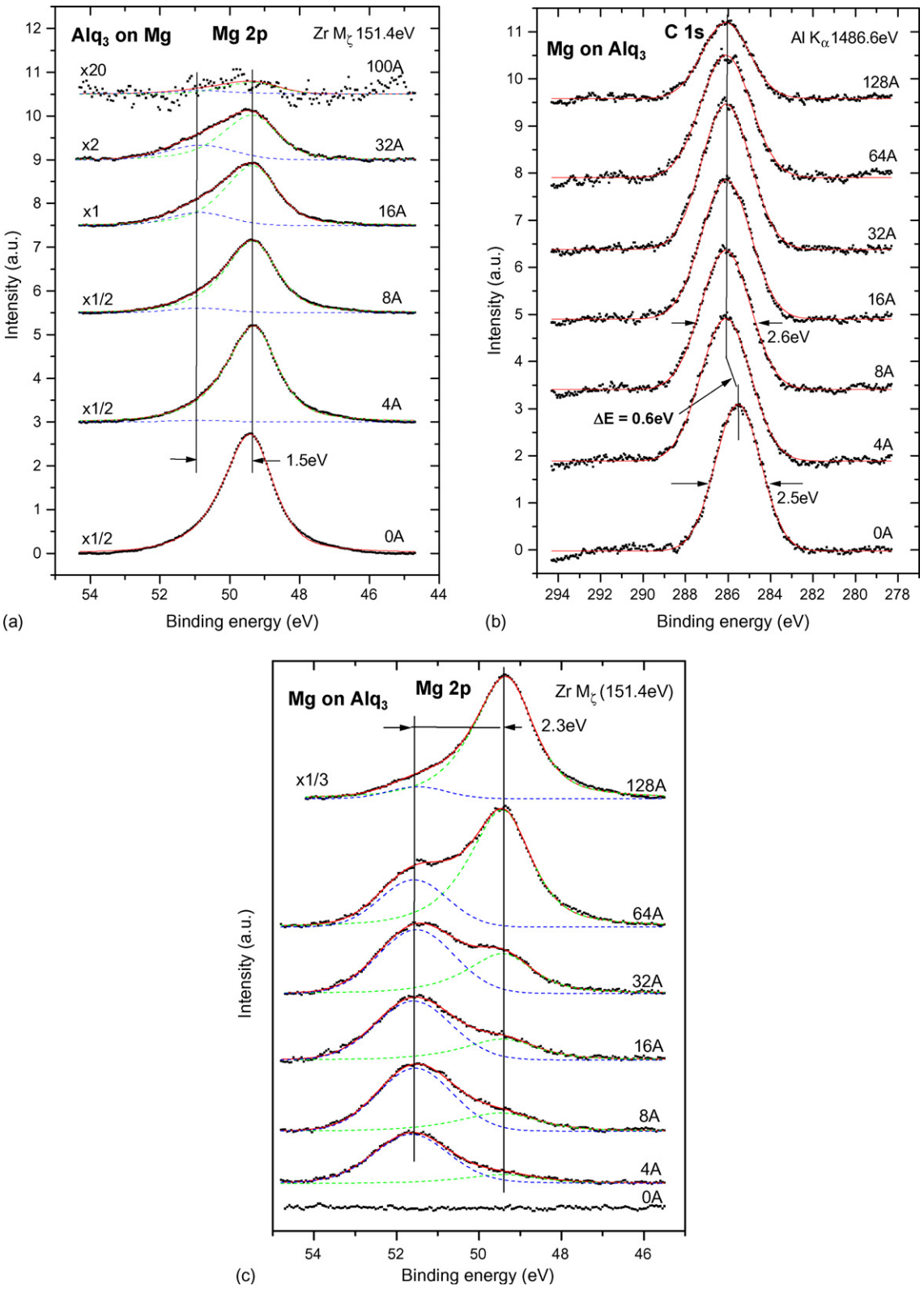

Fig. 29. (a) Mg 2p core level measured as a function of Alq_3 deposition on a clean Mg surface; (b) C 1s and (c) Mg 2p core levels measured as a function of Mg deposition on an Alq_3 film. The rate of decay and binding energy of the core levels suggest very different growth modes of the two interfaces (after [75]).

structures, where the bottom Au surface is again atomically clean (work function ~5.4 eV) prior to molecular deposition, and the top Au contact is vacuum-evaporated. Here again, symmetry in hole-injection is obtained over several orders of magnitude (Fig. 31) [44].

Several comments and conclusions derive from these observations. The first and obvious one is that a difference in interface morphology, such as that observed for Mg-on-Alq_3 vs. Alq_3-on-Mg, does not necessarily imply electrical asymmetry. The vacuum evaporation of a metal on an organic film does not necessarily

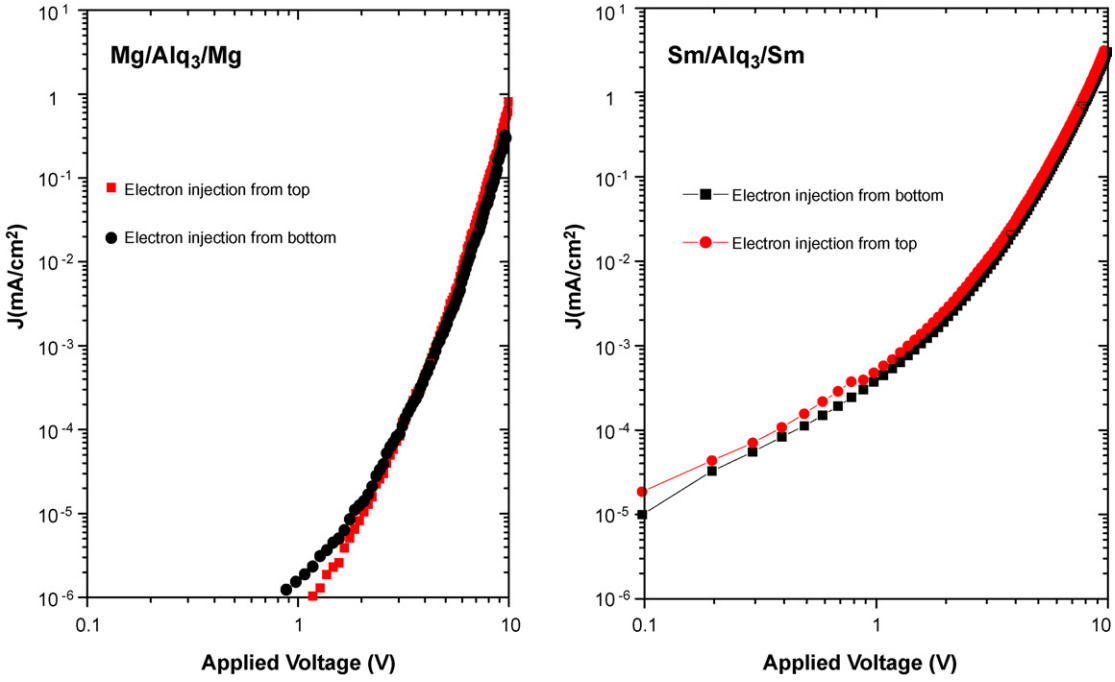

Fig. 30. Current density injected from top (evaporated) and bottom electrodes in $Mg/Alq_3/Mg$ (left) and $Sm/Alq_3/Sm$ (right) structures fabricated in UHV, i.e. on atomically clean metal surfaces. Currents in Alq_3 are unipolar electron currents (after [75]).

create the type ladder-gap states that were thought to help charge carrier injection [137]. The second is that symmetry occurs for both reactive and unreactive interfaces. The Alq_3 cases presented above all involve reactive interfaces. It was originally suggested that the symmetry of top and bottom barriers was due to strong Fermi level pinning on both sides of the organic layer by gap states resulting from metal-Alq_3 chemistry [75]. The Au-α-NPD case dispels this notion, as no evidence of strong chemical interaction is obtained at either top or bottom interface. The third comment concerns the generality of such top vs. bottom contact symmetry. One can anticipate situations whereby top-evaporated metal atoms diffuse into the organic film and create active electronic centers, or act as dopants. Such a situation is encountered with Au atoms that diffuse into per-fluorinated copper phthalocyanine (F_{16}-CuPc) and act as "acceptor states" [138]. F_{16}-CuPc is known as an electron transport materials, in view of the fact that this highly fluorinated molecule has a very low LUMO (EA = 4.5 eV) in which electrons are easily injected. In spite of its large work function, Au (bottom electrode) forms a small electron barrier of ~0.4 eV with F_{16}-CuPc. Yet, the Au/F_{16}-CuPc/Au structure is electrically, in addition to morphologically, asymmetric, with stronger electron injection from the bottom interface. This asymmetry is believed to be due to single Au atoms, or small Au nanoclusters, which diffuse in the top part of the film, act as "doping" centers, and affect the energetics of the top contact [138].

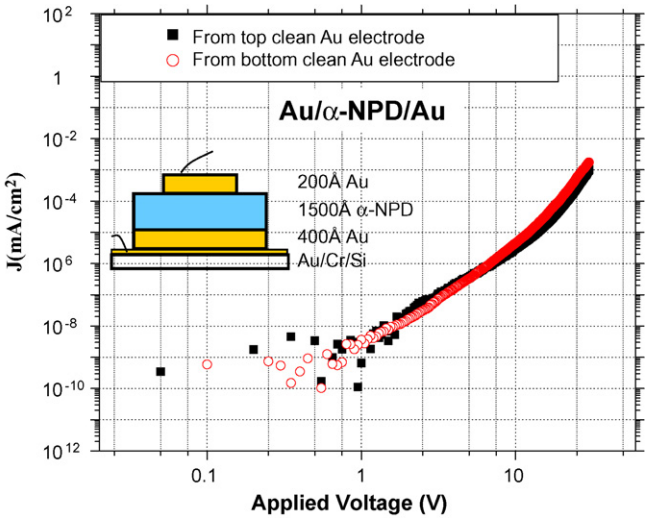

Fig. 31. Current density injected in a Au/α-NPD/Au structure formed in UHV, on an atomically clean Au surface. The current is a unipolar hole current. Red and black data are for holes injected from the bottom and top Au electrodes, respectively (after [44]). (For interpretation of the references to color in this figure legend, the reader is referred to the web version of the article.)

An interface issue that was only recently formally recognized is the impact of the molecular orientation on the IE of the organic film [139,140]. Variations in IE of the order of 0.5 eV, which have been linked to the orientation of molecular crystallites, e.g. lying flat vs. standing up with respect to the organic surface, could have a significant impact on the electronic structure of interfaces. It is unlikely that such an issue arises in the above-mentioned cases of Alq_3 and α-NPD, as these molecules are three-dimensional and form mostly amorphous films. F_{16}-CuPc, on the other hand, is a nearly two-dimensional molecule that is expected to lay nearly flat when in contact with the bottom metal surface, and has been shown to change its orientation in subsequent layers. Variations in IE and molecular level alignment could therefore be an issue with such a compound.

5.2. Molecules on contaminated, or non-metallic, electrodes

Practical organic electronic devices will not be fabricated in high vacuum, and, *a fortiori* not in UHV. Organic-on-electrode structures will therefore comprise metallic, or at least conducting, electrodes that have been exposed to some controlled atmosphere or even ambient air. Non-traditional fabrication techniques such as stamping [141,142], printing [143–145], lamination [122,146,147]

or laser assisted deposition [148,149], which have been shown to be well adapted to organic materials and devices, all involve processing outside of UHV conditions. It is therefore important to review some of the basic differences that have been found between such interfaces and "ideal" interfaces formed under ultra-clean conditions.

Substrate preparation affects composition as well as electrical characteristics of a given surface. Usually, a clean metal surface is a relatively high energy surface, even when reconstructed to minimize surface energy. Molecules of a controlled or ambient atmosphere (N_2, H_2O, CO, O_2, hydrocarbons) adsorb on the surface and partially passivate or oxidize it. This process leads to several differences between clean and exposed metal surfaces. First, the work function of most ambient-exposed metals is reduced, due primarily to the compression of the surface component of the electron wave function, i.e. the pillow effect discussed in Section 2.1.1.2. Second, the contamination, or passivation, layer acts as a physical "spacer", which separates the clean metal from any deposited film. This has crucial consequences for the metal–organic interaction, and affects the interface energetics, molecular orientation and film morphology.

The change in orientation of interface molecules deposited on clean vs. exposed metal surfaces is of importance, as different orientations have been linked to different ionization energy and interface energetics [139,140]. In particular, two-dimensional molecules with delocalized π-electron system generally adsorb in a lying-down configuration on a clean metal surface, and in a standing-up configuration on a contaminated metal, or non-metallic, surface. While we fully recognize the potential impact of the variations, we review here results that include two- as well as three-dimensional molecules, the orientation of which is, in first approximation, independent of the electrode termination.

The molecular level positions at α-NPD and Alq_3 interfaces with atomically clean and contaminated Au surfaces are shown in Figs. 4 and 32 [44,150]. In both cases, the "contaminated" electrode surface was an atomically clean Au surface prepared in UHV and simply exposed for a few minutes to ambient atmosphere. The work function of the exposed Au surface is significantly reduced with respect to that of the clean surface. In terms of interface energetics, the most striking contamination-induced change is the reduction in interface dipole and hole injection barrier. Because of the reduction in interface dipole, the hole barrier is actually smaller with the contaminated, smaller work function, electrode, a result that is somewhat counter-intuitive. The energetics of the contaminated interface are much closer to the Schottky–Mott limit than those of their clean counter-parts. This is also independent of the molecular orientation (α-NPD and Alq_3 are three-dimensional molecules, which are unlikely to take up a specific orientation on the contaminated surface) and chemical interaction with the substrate.

The phenomenon is clearly not limited to "simply exposed" electrode surfaces, but appears to be a general phenomenon that occurs whenever the metal surface is modified from its ultra-clean state. Specific surface treatments, such as ozone-plasma exposure or growth of a SAM to purposely modify the work function, have similar results. The case of α-NPD on ultra-clean vs. ozone treated silver (Ag) [150] is shown in Fig. 33. Ultra-clean Ag has a work function of 4.5 eV, but leads to the formation of a large (0.5 eV) interface dipole, which increases the hole injection barrier. Ozone-treated Ag has a larger work function (5.0 eV), but also leads to a considerably smaller interface dipole of 0.2 eV and a reduced hole barrier (0.7 eV). This "controlled" contamination of the metal surface, i.e. sub-oxide and surface oxygen-related species, also brings the interfaces very close to the Schottky–Mott limit.

The simple metal/organic/metal structures used to test electrical symmetry in organic-on-metal vs. metal-on-organic interfaces are employed here to evaluate the impact of electrode contamination on charge carrier injection. The example of α-NPD deposited on ambient exposed Au and covered with a clean top evaporated contact is shown in Fig. 34 [44]. In contrast with the clean Au/α-NPD/Au sandwich (Fig. 31), the current injected from

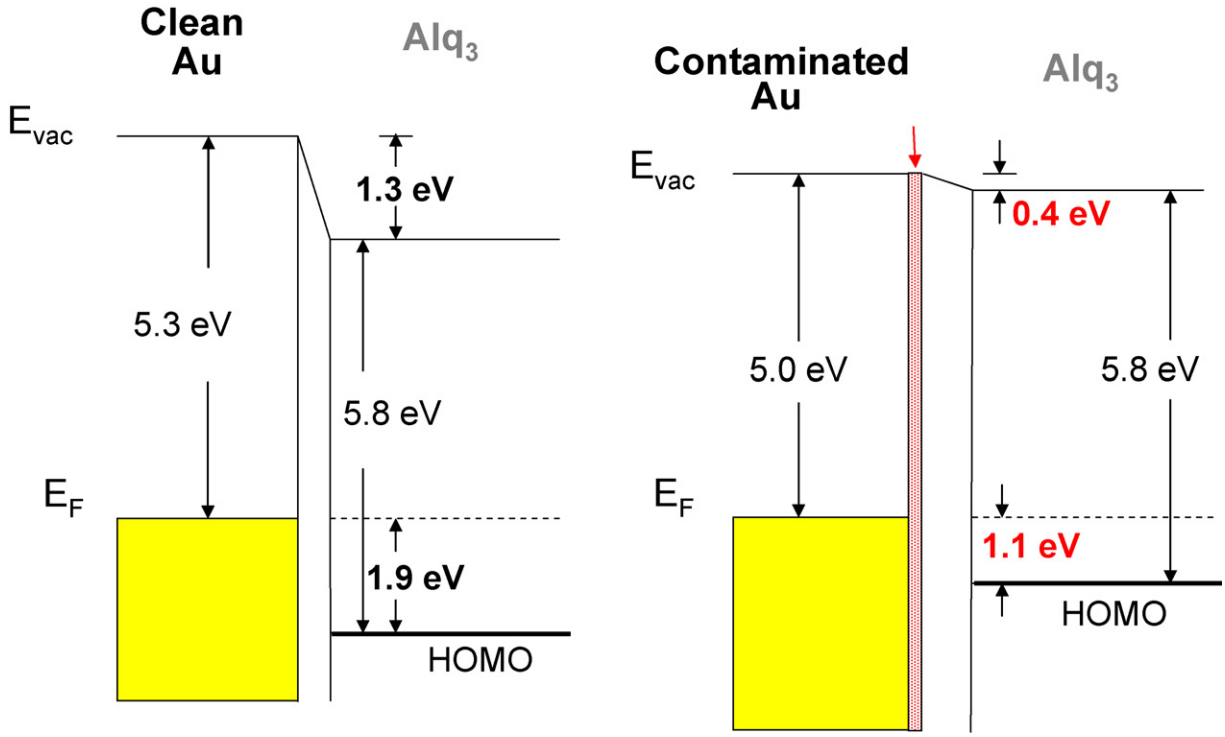

Fig. 32. Comparison of the electronic structure of interfaces formed by vacuum evaporation of Alq_3 on (left) atomically clean Au and (right) contaminated Au, as determined by UPS. Both interface dipole and hole-injection barrier are reduced on the contaminated electrode (after [150]).

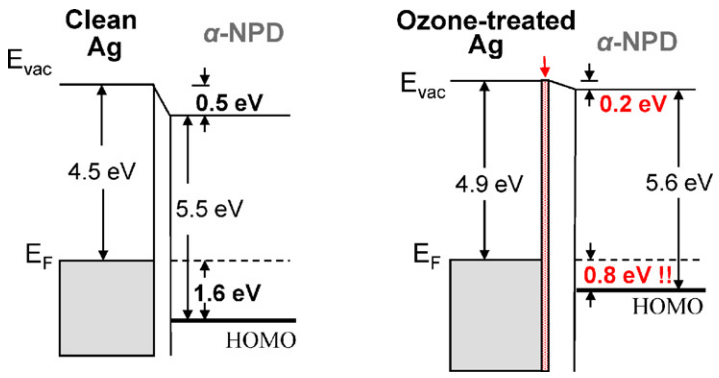

Fig. 33. Comparison of the electronic structure of interfaces formed by vacuum evaporation of α-NPD on (left) atomically clean Ag and (right) ozone-treated Ag, as determined by UPS (after [150]).

the bottom (contaminated) electrode reaches values that are orders of magnitude larger than those of the current injected from the top electrode (the electron injection barriers are larger than 2 eV in both cases, insuring unipolar hole currents in these devices). Note that the current injected from the top Au contact into α-NPD is nearly identical to that injected in the film grown on ultra-clean Au (Fig. 31), suggesting that the morphology and structure of the film are not significantly affected by the electrode contamination. The difference in hole injection is mostly due to the difference in injection barriers (Fig. 32). The case of CuPc sandwiched between air exposed (bottom) and (top evaporated) Au is shown in Fig. 35. Bottom injection yields a current three-to-four orders of magnitude higher than top-injection.

The most significant and counter-intuitive aspect of these results is that the lower work function electrode, i.e. the contaminated Au electrode, yields a lower hole-injection barrier than the higher work function electrode. We attribute this phenomenon to the fact that the organic/metal interaction is profoundly modified by any layer of contamination on the metal, or by the oxygen/oxide in the case of ozone-treated surfaces, and that the reduction in interaction leads to an interface that approaches the Schottky–Mott limit. More insight in this issue is obtained by comparing interfaces between various molecules and metals and non-metals than have similar work functions. A series of such examples are presented in Fig. 36a–c, which compare the energetics of α-NPD, para-sexiphenyl and pentacene on clean Au and PEDOT–PSS [151,152]. Both substrates have very similar work functions (note that variations of these work functions between 4.9 and 5.2 eV are frequently observed in UHV experiments). Remarkably, the hole injection barrier for each molecule is substantially reduced when using PEDOT–PSS, even though the two electrodes have nearly identical work functions. This barrier reduction translates into a several orders of magnitude increase in hole injection (not shown here) [152], a fact that has made PEDOT–PSS a rather popular hole-injecting material in OLEDs, in spite of the drawbacks of chemical instability and limited conductivity.

A summary of the dependence of the hole injection barrier into α-NPD on the work function of clean metal surfaces vs. contaminated and non-metallic surfaces is given in Fig. 37 [150]. The clean metal surfaces lead to a strong departure from the Schottky–Mott limit ($S = 0.5$), presumably due to the mechanisms outlined in Section 2.1 (gap states and pillow effect), whereas the contaminated and non-metallic electrodes do not ($S = 1$). Note that a similar situation has been demonstrated for other molecules, CuPc in particular. One justification of the fact that the energetics of small molecule interfaces with contaminated metallic substrates, or non-metallic conducting substrates, approach the Schottky–Mott limit is that the surface electronic tail, which represents a significant component of the clean metal surface work function, is absent in these cases. On the metallic substrates, the contamina-

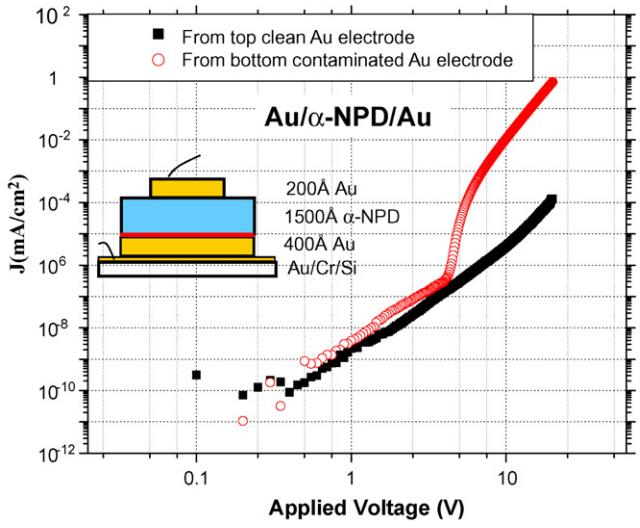

Fig. 34. Same as Fig. 31, for a structure formed in UHV on a contaminated Au surface. The red line on the bottom electrode indicates contamination (after [44]). (For interpretation of the references to color in this figure legend, the reader is referred to the web version of the article.)

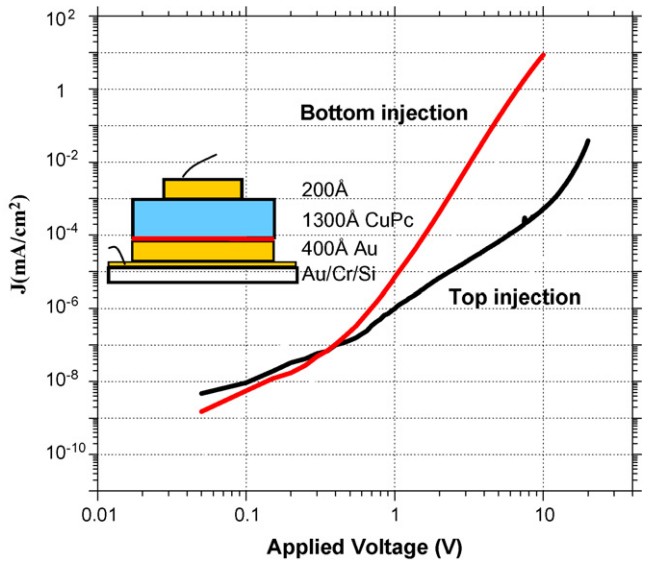

Fig. 35. Same as Fig. 34, for a Au/CuPc/Au structure. The CuPc film thickness is 1300 Å (after [150]).

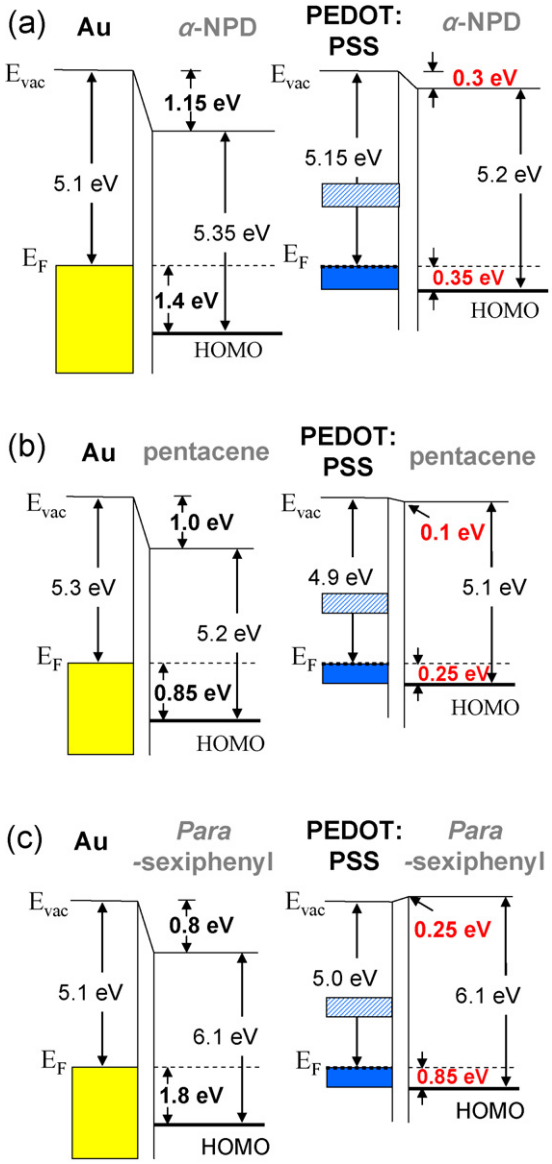

Fig. 36. Comparison of the electronic structure of interfaces formed by UHV deposition of (a) α-NPD, (b) pentacene and (c) para-sexiphenyl on (left) atomically clean Au and (right) PEDOT–PSS, determined by UPS (after [151]).

tion already suppresses this electronic tail. The non-metallic surfaces, like PEDOT–PSS, do not have the metallic character and the electronic density of a standard metal, and the surface electronic tail is not significant. Thus the "pillow effect", i.e. the push-back of the electron tail by the electron density of the adsorbed molecule (Section 2.1.1.2), does not play an important role at interfaces formed on these materials. In some respect, this justification is consistent with the model put forth by the group of S.T. Lee based on the consideration of the metal electronegativity, rather than its work function, in the analysis of organic/metal barriers and interface dipoles [153,154]. The electronegativity is a bulk quantity that is entirely independent of the electronic structure of the surface of the material.

The second justification is based on a reduced interaction between the molecule and the contaminated metal or non-metallic electrode. Section 2.1.2 described interface energetics dominated by interface gap states due to chemical bonding between molecule and metallic electrode [61,64], or to interface gap states originating from the overlap between the continuum of metallic states and the energy gap of the organic semiconductor, i.e. the IDIS [69]. Chemistry is at least modified, if not suppressed, by the passivating contamination layer. The density of IDIS, in particular around the charge neutrality level E_{CNL} of the interface, is strongly reduced by any increase of the effective metal–molecule distance, e.g. by the contamination layer. Consider the UPS spectra of clean Au, contaminated Au and PEDOT–PSS presented in Fig. 38. The analysis of the relative height of the Au Fermi level step on the upper two spectra, assuming an escape depth of ~5–7 Å for the photoemitted electrons, gives an effective contamination layer thickness of 3–5 Å. Thus the effective distance between a molecule deposited on such a contaminated surface and the first plane of metal atoms is expected to increase by that amount, in addition to a possible change in molecular orientation with respect to the metal surface. Vazquez et al. [69] showed that an increase in the PTCDA/Au distance from 2.8 to 3.2 Å diminishes the density of IDIS at the E_{CNL} from 1.5×10^{14} to 0.9×10^{14} eV^{-1} cm^{-2}, nearly a factor of two. The contamination-induced increase in distance of 3–5 Å would necessarily decrease the IDIS by more than an order of magnitude, resulting in weaker interface Fermi level pinning and energetics much closer to the Schottky–Mott limit.

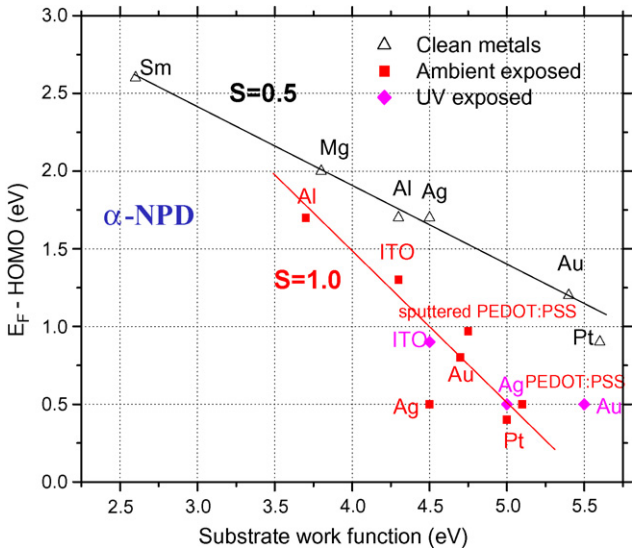

Fig. 37. Hole injection barriers measured by UPS for α-NPD films vacuum-deposited on various ultra-clean metal electrodes (△) and on contaminated metal and non-metal electrodes (■ and ◆). The "clean" interface barriers follow a $S = 0.5$ dependence on the work function, indicating the importance of gap states. The "contaminated" interfaces follow a dependence much closer to the Schottky–Mott limit ($S = 1$) (after [150]).

Interfaces between small molecules and PEDOT–PSS also approach vacuum level alignment (Fig. 36). Greczynski et al. [73,155] and Hwang et al. [156] have used a combination of UPS, XPS and argon ion (Ar^+) sputtering to show that PEDOT–PSS films consists of highly doped grains covered with a 20–30 Å thick insulating PSS shell. The bottom spectrum of Fig. 38 shows a very weak density of states extending to the Fermi level. Removal of the PSS shell via low energy Ar^+ sputtering reveals a much stronger density of states near E_F [41], consistent with the fact that PEDOT–PSS is a heavily p-doped polymer. Yet, the PSS shell at the interface between small molecules and the PEDOT–PSS surface separates the molecules from the large density of states of the substrate, playing a similar role to that of the contamination layer on the metal surface. The molecule–substrate interaction is reduced, and the interface energetics approach the Schottky–Mott limit.

6. Conclusions: a unified picture

It is clear that commercial organic electronic device fabrication demands processing conditions that are far from the ultra-clean conditions afforded by UHV environment. It is also very clear, however, that the UHV-surface/interface science work done on ultra-clean and controllably contaminated organic interfaces done by a number of groups around the world in the past decade has led to a far better understanding of the basic mechanisms that control these interfaces. It has allowed us to distinguish intrinsic from extrinsic mechanisms, and obtain a unified interface picture. It is therefore in this context that we wrote this review article, with two main goals in mind. The first was to describe a series of results obtained in the past 3 years on polymer and small molecule interfaces with various electrode materials, emphasizing the differences and similarities between organic-on-top and electrode-on-top interfaces as well as the role of electrode contamination in the interface electronic structure. The second goal was to establish whether intrinsic differences exist between the mechanisms that govern the energetics of small molecule and polymer interfaces.

The results presented in this review clearly show that a critical issue, when considering molecular level alignment at metal–organic interfaces, is whether the interface is formed between the organic film and an atomically clean metal surface, or between the organic film and a "contaminated" metal surface or a non-metallic conducting surface. The former case is encountered when a molecular film is evaporated in UHV on an atomically clean metal surface, or when a metal contact is vacuum-evaporated on a molecular or polymer films. An intimate metal–organic interface is then formed, and the interface energetics are found to depart from the Schottky–Mott limit. A dipole is often present at such an interface, due either to the "pillow effect" or to interface electronic gap states due to chemistry or induced by the metal. The latter case is encountered when a molecular film is evaporated on a "contaminated", or "passivated", metal surface, or when a polymer film is spun from liquid phase on an ambient-exposed metal surface. In these cases, the organic–substrate interaction is suppressed, or at least greatly diminished, leading to interface energetics that closely follow the Schottky–Mott limit. Similar results are obtained with non-metallic electrodes, such as the conducting polymer PEDOT–PSS, which are generally less reactive than metals and/or do not exhibit the large electronic

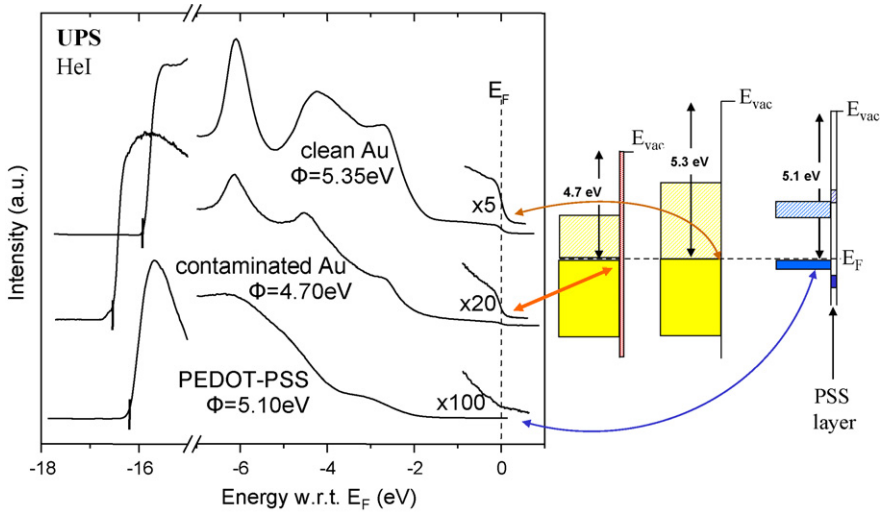

Fig. 38. (Left) UPS spectra of valence states and Fermi level region of (top) atomically clean Au, (middle) contaminated Au, and (bottom) PEDOT–PSS. Work functions are indicated. (Right) Schematics of the corresponding electronic structures, showing the effect of the Au contamination layer and PSS shell.

density of their metallic counterparts. Injection barriers at such interfaces can generally be predicted from the organic semiconductor parameters, i.e. ionization energy and electron affinity, and the electrode work function, assuming that it is independently measured.

Based on these simple rules, we conclude that differences in electronic structure and electrical behavior between organic-on-metal and metal-on-organic are nearly entirely grounded on the environmental context of the interface formation. Except in specific cases where diffusion of metal species evaporated on an organic film leads to electrical doping of the film, a metal/organic/metal sandwich structure made in UHV behaves symmetrically, i.e. charge injection is identical from top and bottom contacts. On the other hand, the same structure made with a contaminated bottom metal surface, which is unavoidable because of processing in the case of a polymer structure, behaves asymmetrically, generally with higher hole injection (lower hole injection barrier) from the bottom contaminated interface. The data do not generally support the notion of intermediate gap states that help injection in the case of an evaporated metal-on-organic contact. Data on "contaminated metal" interfaces are also highly relevant to all processing techniques involving printing, stamping and lamination of device components, e.g. top contacts, which necessarily involve surfaces that have been exposed to controlled, or ambient, atmosphere.

Finally, we find no fundamental differences between molecular level alignment behavior at small molecule and polymer interfaces. We suggest, here again, that any perceived differences, such as the observed interface dipole for the former and the Schottky–Mott limit for the latter, are the product of environmental conditions, as stated above. "Clean" metal–polymer interfaces, obtained by vacuum evaporation of top contacts, depart from the Schottky–Mott limit, as do their small molecule counterparts formed on clean metal surfaces. "Contaminated" polymer–metal interfaces, obtained by normal spin-coating, closely follow the Schottky–Mott limit, as do their small molecule counterparts formed on contaminated metal surfaces. Both types of interfaces display the normal Fermi level pinning when the electrode work function spans out of the semiconductor gap, although the pinning position and mechanism remains somewhat of an open question.

We hope that these data and considerations will help researchers in the field of organic devices rationalize somewhat the way they approach the modeling of organic–electrode interfaces.

Acknowledgements

The work reviewed in this paper was supported over the past few years by the U.S. Department of Energy (DE-FG02-04ER46165), the National Science Foundation (DRM-0408589 and 0705920) and the Princeton MRSEC of the National Science Foundation (DMR-0213706). The authors are very grateful to Profs. Jean-Luc Brédas, Fernando Flores, Zoltan Soos and Jeffrey Schwartz for key collaborations in the areas of electronic structure of polymer and small molecules, interface gap states, polarization and exciton binding energy, and interface modification and chemistry, respectively. AK also gratefully acknowledges former members of the group, Profs. Norbert Koch, Ian Hill, and Chi-I Wu, and Drs. Yutaka Hirose, Chongfei Shen, Weying Gao and Calvin Chan, who all participated at some point in time in some of these experiments.

Finally, the authors note with great sadness the recent passing of Professor Kazuhiko Seki, Nagoya University, a pioneer in the field of organic thin film interfaces. Much of the current work on organic interfaces was inspired from his and his colleagues' insightful work done in the 1980s and 1990s on electron spectroscopy on organic thin films. With his untimely death, our community has lost an internationally recognized and respected scholar and a wonderful gentleman.

References

[1] C.W. Tang, S.A. Vanslyke, Appl. Phys. Lett. 51 (1987) 913.
[2] J.H. Burroughes, D.D.C. Bradley, A.R. Brown, R.N. Marks, K. Mackay, R.H. Friend, P.L. Burns, A.B. Holmes, Nature 347 (1990) 539.
[3] J.R. Sheats, H. Antoniadis, M. Hueschen, W. Leonard, J. Miller, R. Moon, D. Roitman, A. Stocking, Science 273 (1996) 884.
[4] M.A. Baldo, D.F. O'Brien, Y. You, A. Shoustikov, S. Sibley, M.E. Thompson, S.R. Forrest, Nature 395 (1998) 151–154.
[5] R.H. Friend, R.W. Gymer, A.B. Holmes, J.H. Burroughes, R.N. Marks, C. Taliani, D.D.C. Bradley, D.A. Dos Santos, J.-L. Bredas, M. Logdlund, W.R. Salaneck, Nature 397 (1999) 121–128.
[6] C. Adachi, M.A. Baldo, M.E. Thompson, S.R. Forrest, J. Appl. Phys. 90 (2001) 5048.
[7] B.W. D'Andrade, J. Brooks, V. Adamovich, M.E. Thompson, S.R. Forrest, Adv. Mater. 14 (2002) 1032–1036.
[8] G.B. Blanchet, Y.-L. Loo, J.A. Rogers, F. Gao, C.R. Fincher, Appl. Phys. Lett. 82 (2003) 463.
[9] T. Someya, Y. Kato, I. Shingo, Y. Noguchi, T. Sekitani, H. Kawaguchi, T. Sakurai, IEEE Trans. Electron Devices 52 (2005) 2502–2511.
[10] T. Sekitani, M. Takamiya, Y. Noguchi, S. Nakano, Y. Kato, T. Sakurai, T. Someya, Nat. Mater. 6 (2007) 413–417.
[11] J.J.M. Halls, C.A. Walsh, N.C. Greenham, E.A. Marseglia, R.H. Friend, S.C. Moratti, A.B. Holmes, Nature 376 (1995) 6540.
[12] G. Yu, J. Gao, J.C. Hummelen, F. Wudl, A.J. Heeger, Science 270 (1995) 1789.
[13] P. Peumans, V. Bulovic, S.R. Forrest, Appl. Phys. Lett. 76 (2000) 2650.
[14] P. Peumans, S.R. Forrest, Appl. Phys. Lett. 79 (2001) 126–128.
[15] S.E. Shaheen, C.J. Brabec, N.S. Sariciftci, F. Padinger, T. Fromherz, J.C. Hummelen, Appl. Phys. Lett. 78 (2001) 841.
[16] F. Padinger, R.S. Rittberger, N.S. Sariciftci, Adv. Funct. Mater. 13 (2003) 85–88.
[17] J. Xue, S. Uchida, B.P. Rand, S.R. Forrest, Appl. Phys. Lett. 85 (2004) 5757.
[18] M.C. Scharber, D. Wuhlbacher, M. Koppe, P. Denk, C. Waldauf, A.J. Heeger, C.J. Brabec, Adv. Mater. 18 (2006) 789.
[19] F. Yang, M. Shtein, S.R. Forrest, Nat. Mater. 4 (2005) 37–41.
[20] P. Harrop, R. Das, Organic Electronics Forecasts, Players & Opportunities 2005–2025, in: ID techEx, 2006.
[21] Y. Kato, T. Sekitani, M. Takamiya, M. Doi, K. Asaka, T. Sakurai, T. Someya, IEEE Trans. Electron Devices 54 (2007) 202–209.
[22] J.Y. Kim, K. Lee, N.E. Coates, D. Moses, T.-Q. Nguyen, M. Dante, A.J. Heeger, Science 317 (2007) 222.
[23] R. Nolan, NanoMarket LC (2006).
[24] M. Pope, C. Swenberg, Electronic Process in Organic Crystals and Polymers, Oxford University Press, Oxford, 1999.
[25] E.A. Silinsh, Organic Molecular Crystals, Their Electronic States, Springer-Verlag, Berlin, 1980.
[26] C.B. Duke (Ed.), The Electronic Structure of Semiconducting Polymers, Plenum Press, New York, 1982, pp. 59–125.
[27] V.I. Adamovich, S.R. Codero, P.I. Djurovich, A. Tamayo, M.E. Thompson, B. D'Andrade, S.R. Forrest, Org. Electron. 4 (2003) 77–87.
[28] C.W. Tang, S. Slyke, Appl. Phys. Lett. 51 (1987) 913.
[29] S.R. Forrest, P.E. Burrows, Z. Shen, G. Gu, V. Bulovic, M.E. Thompson, Synth. Met. 91 (1997) 9.
[30] E.A. Silinish, V. Capek, Organic Molecular Crystals, AIP Press, New York, 1994.
[31] N.W. Ashcroft, N.D. Mermin, Solid State Physics, Saunder College Publishing, 1976.
[32] I.H. Campbell, S. Rubin, T.A. Zawodzinski, J.D. Kress, R.L. Martin, D.L. Smith, N.N. Barashkov, J.P. Ferraris, Phys. Rev. B 54 (1996) R14321.
[33] Y. Vaynzof, T.J. Dennes, J. Schwartz, A. Kahn, Appl. Phys. Lett. 93 (2008) 103305.
[34] H. Lee, S.W. Cho, K. Han, P.E. Jeon, C.N. Whang, K. Jeong, K. Cho, Y. Yi, Appl. Phys. Lett. 93 (2008) 043308.
[35] J. Blochwitz, T. Fritz, M. Pfeiffer, K. Leo, D.M. Alloway, P.A. Lee, N.R. Armstrong, Org. Electron. 2 (2001) 97.
[36] W. Gao, A. Kahn, Appl. Phys. Lett. 79 (2001) 4040.
[37] S.Z. Sze, Physics of Semiconductor Devices, 2nd ed., Wiley, New York, 1981.
[38] E.H. Rhoderick, R.H. Williams, Metal-Semiconductor Contacts, Oxford, 1988.
[39] W. Mönch, Semiconductor Surfaces and Interfaces, Springer-Verlag, Berlin/Heidelberg, 1993.
[40] C. Tengstedt, W. Osikowicz, W.R. Salaneck, I.D. Parker, C.H. Hsu, M. Fahlman, Appl. Phys. Lett. 88 (2006) 053502.
[41] J. Hwang, E.-G. Kim, J. Liu, J.-L. Brédas, A. Duggal, A. Kahn, J. Phys. Chem. 111 (2007) 1378.
[42] M. Lögdlund, T. Kugler, G. Greczynski, A. Crispin, W. Salaneck, M. Fahlman, in: W.R. Salaneck, K. Seki, A. Kahn, J.-J. Pireaux (Eds.), Conjugated Polymer and Molecular Interfaces, Marcel Dekker, Inc., 2001, p. 73.
[43] I.H. Campbell, J.P. Ferraris, T.W. Hagler, M.D. Joswick, I.D. Parker, D.L. Smith, Polym. Adv. Technol. 8 (1997) 417.
[44] A.S. Wan, J. Hwang, F. Amy, A. Kahn, Org. Electron. 6 (2005) 47.
[45] C. Shen, A. Kahn, I.G. Hill, in: W.R. Salaneck, K. Seki, A. Kahn, J.-J. Pireaux (Eds.), Conjugated Polymer and Molecular Interfaces, Marcel Dekker, Inc., 2001, p. 351.
[46] H. Ishii, K. Seki, IEEE Trans. Electron Devices 44 (1997) 1295.
[47] I. Hill, A. Kahn, J. Appl. Phys. 84 (1998) 5583.
[48] X. Crispin, V. Geskin, A. Crispin, J. Cornill, R. Lazzaroni, W.R. Salaneck, J.L. Brédas, J. Am. Chem. Soc. 124 (2002) 8131.
[49] A. Kahn, N. Koch, W. Gao, J. Polym. Sci., Polym. Phys. 41 (2003) 2529.
[50] Y.C. Chen, et al. Phys. Rev. B (1984) 30.
[51] H. Ishii, K. Sugiyama, E. Ito, K. Seki, Adv. Mater. 11 (1999) 605.
[52] P. Bagus, V. Staemmler, C. Wöll, Phys. Rev. Lett. 89 (2002) 096104.

[53] L.J. Brillson, Surf. Sci. Rep. 2 (1982) 123.
[54] W. Mönch, Rep. Prog. Phys. 53 (1990) 221–278.
[55] W.E. Spicer, I. Lindau, P.E. Gregory, C.M. Garner, P. Pianetta, P.W. Chye, J. Vac. Sci. Technol. 13 (1976) 780.
[56] W.E. Spicer, P.W. Chye, P.R. Skeath, C.Y. Su, I. Lindau, J. Vac. Sci. Technol. 16 (1979) 1422.
[57] W.E. Spicer, Z. Liliental-Weber, E. Weber, N. Newman, T. Kendelewicz, R. Cao, C. McCants, P. Mahowald, K. Miyano, I. Lindau, J. Vac. Sci. Technol. B 6 (1988) 1245–1251.
[58] V.E. Choong, M.G. Mason, C.W. Tang, Y. Gao, Appl. Phys. Lett. 72 (1998) 2689.
[59] M.G. Mason, C.W. Tang, L.S. Hung, P. Raychaudhuri, J. Madathil, D.J. Giesen, L. Yan, Q.T. Le, Y. Gao, S.T. Lee, L.S. Liao, L.F. Cheng, J. Appl. Phys. 89 (2001) 2756.
[60] N.J. Watkins, A.J. Makinen, Y. Gao, M. Uchida, Z.H. Kafafi, J. Appl. Phys. 100 (2006) 103706.
[61] S. Meloni, A. Palma, J. Schwartz, A. Kahn, R. Car, J. Am. Chem. Soc. 125 (2003) 7808.
[62] C. Shen, I.G. Hill, A. Kahn, J. Schwartz, J. Am. Chem. Soc. 122 (2000) 5391.
[63] C. Shen, A. Kahn, J. Schwartz, J. Appl. Phys. 89 (2001) 449.
[64] C. Shen, A. Kahn, Org. Electron. 2 (2001) 89.
[65] V. Heine, Phys. Rev. 138 (1965) A1689.
[66] S.G. Louie, H. Cohen, Phys. Rev. B 13 (1976) 2461.
[67] C. Tejedor, E. Louis, F. Flores, J. Phys. C: Solid State Phys. 10 (1977) 2163.
[68] W. Mönch, Surf. Sci. 299 (1994) 928.
[69] H. Vazquez, R. Oszwaldowski, P. Pou, J. Ortega, R. Perez, F. Flores, A. Kahn, EuroPhys. Lett. 65 (2004) 802.
[70] H. Vazquez, F. Flores, R. Oszwaldowski, J. Ortega, R. Perez, A. Kahn, Appl. Surf. Sci. 234 (2004) 107.
[71] H. Vazquez, Y.J. Dappe, J. Ortega, F. Flores, J. Chem. Phys. 126 (2007) 144703.
[72] I. Hill, A. Rajagopal, A. Kahn, Y. Hu, Appl. Phys. Lett. 73 (1998) 662.
[73] G. Greczynski, T. Kugler, W.R. Salaneck, Thin Solid Films 354 (1999) 129.
[74] Y. Hirose, A. Kahn, V. Aristov, P. Soukiassian, V. Bulovic, S.R. Forrest, Phys. Rev. B 54 (1996) 13748.
[75] C. Shen, A. Kahn, J. Schwartz, Appl. Phys. 89 (2001) 449.
[76] I.H. Campbell, D.L. Smith, Appl. Phys. Lett. 74 (1999) 561.
[77] J. Hwang, A. Kahn, in: Z. Kafafi, F. So (Eds.), SPIE, Organic Light Emitting Materials and Devices, vol. 6333, SPIE, 2006.
[78] H. Lüth, Surfaces and Interfaces of Solids, Springer-Verlag, Berlin/Heidelberg, 1993.
[79] J.E. Rowe, S.B. Christman, E.E. Chaban, Rev. Sci. Instrum. 44 (1973) 1675.
[80] R. Avci, Q. Cai, G.J. Lapeyre, Rev. Sci. Instrum. 60 (1989) 3643.
[81] C. Wu, Y. Hirose, H. Sirringhaus, A. Kahn, Chem. Phys. Lett. 272 (1997) 43.
[82] P.T. Andrews, I.R. Collins, J.E. Ingelsfield (Eds.), Unoccupied Electronic States, Springer-Verlag, 1992.
[83] S. Barlow, Q. Zhang, B.R. Kaafarani, C. Risko, F. Amy, C.K. Chan, B. Domercq, Z.A. Starikova, M.Y. Antipin, T.V. Timofeeva, B. Kippelen, J.-L. Brédas, A. Kahn, S.R. Marder, Chem. Eur. J. 13 (2007) 3537–3547.
[84] N. Sato, K. Seki, H. Inokuchi, J. Chem. Soc. 77 (1981) 1621.
[85] I.G. Hill, A. Kahn, G. Soos, A. Pascal, Chem. Phys. Lett. 327 (2000) 181.
[86] J.H. Weaver, J. Phys. Chem. Solids 53 (1992) 1433.
[87] J.H. Weaver, D.M. Poirier, in: E. Ehrenreich, F. Spaepen (Eds.), Solid State Physics Series, vol. 48, Academic Press, New York, 1994.
[88] C.I. Wu, Y. Hirose, H. Sirringhaus, A. Kahn, Chem. Phys. Lett. 272 (1997) 43.
[89] D.R.T. Zahn, G.N. Gavrila, M. Gorgoi, Chem. Phys. 325 (2006) 99–112.
[90] S. Krause, M.B. Casu, A. Scholl, E. Umbach, New J. Phys. 10 (2008) 085001.
[91] G. Gerstenblum, J.-J. Pireaux, P.A. Thiry, R. Caudano, J.P. Vigneron, P. Lambin, A.A. Lucas, W. Krätschmer, Phys. Rev. Lett. 67 (1991) 2171.
[92] R.W. Lof, M.A. van Veenendal, B. Koopmans, H.T. Jonkman, G.A. Sawatzky, Phys. Rev. Lett. 68 (1992) 3924.
[93] D. Cahen, A. Kahn, Adv. Mater. 15 (2003) 271.
[94] E.M. Conwell, Synth. Met. 83 (1996) 101.
[95] A.J. Cadby, P.A. Lane, M. Wohlgenannt, C. An, Z.V. Vardeny, D.D.C. Bradley, Synth. Met. 111 (2000) 515.
[96] W.R. Salaneck, S. Stafström, J.L. Brédas (Eds.), Conjugated Polymer Surfaces and Interfaces, Cambridge University Press, Cambridge, 1996.
[97] G. Greczynski, M. Fahlman, W. Salaneck, N. Johanson, D.A. Dos Santos, A. Dkhissi, J.L. Brédas, J. Chem. Phys. 116 (2002) 1700.
[98] M. Ariu, D.G. Lidzey, D.D.C. Bradley, Synth. Met. 111/112 (2000) 607.
[99] J.S. Kim, R.H. Friend, I. Grizz, J.H. Burroughes, Appl. Phys. Lett. 87 (2005) 023506.
[100] W.R. Salaneck, M. Lögdlund, M. Fahlman, G. Greczynski, T. Kugler, Mater. Sci. Eng. Rep. 34 (2001) 121–146.
[101] J.L. Brédas, R.R. Chance, R. Silbey, J. Chem. Phys. 75 (1981) 255.
[102] J. Cornil, S. Vanderdonckt, R. Lazzaroni, D.A. Santos, G. Thys, H.J. Geise, L.-M. Yu, M. Szablewski, D. Bloor, M. Lögdlund, W.R. Salaneck, N.E. Gruhn, D.L. Lichtenberger, P.A.A. Lee, N.R.J.L. Brédas, Chem. Mater. 11 (1999) 2436.
[103] J.C. Sancho-Garcia, C.L. Foden, I. Grizz, G. Greczynski, M.P. de Jong, W.R. Salaneck, J.L. Brédas, J. Cornil, J. Phys. Chem. B 108 (2004) 5594–5599.
[104] J. Hwang, in: Electrical Engineering, vol. Ph.D., Princeton University, Princeton, 2007, p. 141.
[105] W.R. Salaneck, Phys. Rev. Lett. 40 (1978) 60.
[106] M. Knupfer, J. Fink, E. Zojer, G. Leising, D. Fichou, Chem. Phys. Lett. 318 (2000) 585.
[107] M. Knupfer, Appl. Phys. A 77 (2003) 623–626.
[108] S. Möller, G. Weiser, C. Lapersonne-Meyer, Synth. Met. 116 (2001) 23.
[109] S. Kera, N. Ueno, Proc. Int. Symp. Super-Functionality Org. Dev. IPAP Conf. Series 6, 2005, 51–56.
[110] E.V. Tsiper, Z.G. Soos, W. Gao, A. Kahn, Chem. Phys. Lett. 360 (2002) 47.
[111] E.V. Tsiper, Z.G. Soos, Phys. Rev. B 68 (2003) 085301.
[112] H. Yamane, S. Nagamatsu, H. Fukagawa, S. Kera, R. Friedlein, K.K. Okudaira, N. Ueno, Phy. Rev. B 72 (2005) 153412.
[113] G. Gensterblum, J.-J. Pireaux, P.A. Thiry, R. Caudano, T. Buslaps, R.L. Johnson, G. Le Lay, V. Aristov, R. Gunther, A. Taleb-Ibrahimi, G. Indlekofer, Y. Petroff, Phys. Rev. B 48 (1993) 14756.
[114] S. Hasegawa, T. Mori, K. Imaeda, S. Tanaka, Y. Yamashitam, H. Ionkuchi, H. Fujimoto, K. Seki, N. Ueno, J. Chem. Phys. 100 (1994) 6969.
[115] H.H. Fong, P.A.G. Malliaras, Appl. Phys. Lett. 89 (2006) 172116.
[116] I.N. Hulea, H.B. Brom, A.J. Houtepen, D. Vanmaekelbergh, J.J. Kelly, E.A. Meulenkamp, Phys. Rev. Lett. 93 (2004) 166601.
[117] O. Tal, Y. Rosenwaks, Y. Preezant, N. Tessler, C.K. Chan, A. Kahn, Phys. Rev. Lett. 95 (2005) 256405.
[118] K. Celebi, P.J. Jadhav, K.M. Milaninia, M. Bora, M.A. Baldo, Appl. Phys. Lett. 93 (2008) 083308.
[119] H. Ishii, K. Sugiyama, D. Yoshimura, E. Ito, Y. Ouchi, K. Seki, IEEE J. Sel. Top. Quantum Electron. 4 (1998) 24.
[120] H. Peisert, M. Knupfer, J. Fink, Appl. Phys. Lett. 81 (2002) 2400.
[121] M. Fahlman, A. Crispin, X. Crispin, S.K.M. Henze, M.P. de Jong, W. Osikowicz, C. Tengstedt, W.R. Salaneck, J. Phys.: Condens. Matter 19 (2007) 183202.
[122] J. Liu, L.N. Lewis, T.J. Faircloth, A.R. Duggal, Appl. Phys. Lett. 88 (2006) 223509.
[123] Y. Vaynzof, T.J. Dennes, J. Schwartz, A. Kahn, in preparation.
[124] F.J. Zhang, A. Vollmer, J. Zhang, C. Xu, J.P. Rabe, N. Koch, Org. Electron. 8 (2007) 606.
[125] M. Kemerink, J.M. Kramer, H.H.P. Gommans, R.A.J. Janssen, Appl. Phys. Lett. 88 (2006) 192108.
[126] M.H. Hecht, J. Vac. Sci. Technol. B 8 (1990) 1018.
[127] M. Alonso, R. Cimino, K. Horn, Phys. Rev. Lett. 64 (1990) 1947.
[128] D. Mao, A. Kahn, M. Marsi, G. Margaritondo, Phys. Rev. B 42 (1990) 3228.
[129] L. Kronik, Y. Shapira, Surf. Sci. Rep. 37 (1999) 1–206.
[130] K. Seki, N. Hayashi, H. Oji, Thin Solid Films 393 (2001) 298.
[131] N. Koch, A.C. Dürr, J. Ghijsen, R.L. Johnson, J.-J. Pireaux, J. Schwartz, A. Kahn, Thin Solid Films 441 (2003) 145.
[132] C. Shen, I.G. Hill, A. Kahn, Adv. Mater. 11 (1999) 1523.
[133] H. Ishii, K. Sugiyama, E. Ito, Adv. Mater. 11 (1999) 605.
[134] I.H. Campbell, D.L. Smith, in: W.R. Salaneck, K. Seki, A. Kahn, J.-J. Pireaux (Eds.), Conjugated Polymer and Molecular Interfaces, Marcel Dekker, Inc., 2001, p. 693.
[135] I.H. Cambell, D.L. Smith, Solid State Phys. 55 (2001) 1–117.
[136] V. Bulovic, in: Electrical Engineering, vol. Ph.D., Princeton University, 1998.
[137] G. Parthasarathy, P.E. Burrows, V. Khalfin, V.G. Kozlov, S.R. Forrest, Appl. Phys. Lett. 72 (1998) 2138.
[138] C. Shen, A. Kahn, J. Appl. Phys. 90 (2001) 4549.
[139] S. Duhm, G. Heimel, I. Salzmann, H. Glowatzki, R.L. Johnson, A. Vollmer, J.P. Rabe, N. Koch, Nat. Mater. 7 (2008) 326–332.
[140] I. Salzmann, S. Duhm, G. Heimel, M. Oehzelt, R. Kniprath, R.L. Johnson, J.P. Rabe, N. Koch, J. Am. Chem. Soc. 130 (2008) 12870–12871.
[141] C. Kim, P.E. Burrows, S.R. Forrest, Science 288 (2000) 831–833.
[142] C. Kim, M. Shtein, S.R. Forrest, Appl. Phys. Lett. 80 (2002) 4051–4053.
[143] T.B. Hebner, C.C. Wu, D. Marcy, M.H. Lu, J.C. Sturm, Appl. Phys. Lett. 72 (1998) 519–521.
[144] H. Sirringhaus, T. Kawase, R.H. Friend, T. Shimoda, M. Inbasekaran, W.W. Wu, E.P. Woo, Science 290 (2000) 2123.
[145] T. Kawase, T. Shimoda, C. Newsome, H. Sirringhaus, R.H. Friend, Thin Solid Films 438 (2003) 279–287.
[146] Y.-L. Loo, T. Someya, K.W. Baldwin, Z. Bao, P. Ho, A. Dodabalapur, H.E. Katz, J.A. Rogers, Proc. Natl. Acad. Sci. U.S.A. 99 (2002) 10252–10256.
[147] D.A. Bernards, T. Biegala, Z.A. Samuels, J.D. Slinker, G. Malliaras, S.F. Torres, H.D. Abruna, J.A. Rogers, Appl. Phys. Lett. 84 (2004) 3675–3677.
[148] B. Toftmann, M.R. Papantonakis, R.C.Y. Auyeung, W. Kim, S.M. O'Malley, D.M. Bubb, J.S. Horwitz, J. Schou, P.M. Johansen, R.F.J. Haglund, Thin Solid Films 453 (2004) 177–181.
[149] C.B. Arnold, A. Piqué, MRS Bull. 32 (2007) 9–12.
[150] A.S.-C. Wan, in: Electrical Engineering, vol. Ph.D., Princeton University, Princeton, 2006.
[151] N. Koch, J. Ghijsen, A. Elschner, R.L. Johnson, J.-J. Pireaux, J. Schwartz, A. Kahn, Appl. Phys. Lett. 82 (2003) 70.
[152] N. Koch, A. Elschner, J. Schwartz, A. Kahn, Appl. Phys. Lett. 82 (2003) 2281.
[153] J.X. Tang, C.S. Lee, S.T. Lee, Y.B. Xu, Chem. Phys. Lett. 396 (2004) 92–96.
[154] J.X. Tang, C.S. Lee, S.T. Lee, Appl. Phys. Lett. 87 (2005) 252110.
[155] G. Greczynski, T. Kugler, M. Keil, W. Osikowicz, M. Falman, W.R. Salaneck, J. Electron. Spectrosc. Relat. Phenom. 121 (2001) 1.
[156] J. Hwang, F. Amy, A. Kahn, Org. Electron. 7 (2006) 387.
[157] C.K. Chan, W. Zhao, S. Barlow, S.R. Marder, A. Kahn, Org. Electron. 9 (2008) 575.
[158] P.G. Schroeder, C.B. France, J.B. Park, B.A. Parkinson, J. Appl. Phys. 91 (2002) 3010–3014.
[159] N. Koch, J. Ghijsen, R.L. Johnson, J. Schwartz, J.-J. Pereaux, A. Kahn, J. Phys. Chem. B 106 (2002) 4192.
[160] C.K. Chan, A. Kahn, Appl. Phys. A, 2008, in press.
[161] E.-G. Kim, J.L. Brédas, private communication.